EVOLUTIONARY STRUCTURAL OPTIMIZATION WITH MULTIPLE PERFORMANCE CONSTRAINTS BY LARGE ADMISSIBLE PERTURBATIONS

by

Taemin Earmme

A dissertation submitted in partial fulfillment
of the requirements for the degree of
Doctor of Philosophy
(Mechanical Engineering and Naval Architecture and Marine Engineering)
in The University of Michigan
2009

Doctoral Committee:

Professor Michael M. Bernitsas, Co-Chair
Professor Panos Y. Papalambros, Co-Chair
Professor Armin W. Troesch
Associate Professor Dale G. Karr

To My Parents

ACKNOWLEDGEMENTS

I would like to thank my advisor, Professor Michael Bernitsas for his valuable advice and guidance throughout my graduate work. I also like to express sincere appreciation to the members of my dissertation committee, Professor Papalambros, Professor Troesch and Professor Karr, especially thankful to Professor Papalambros who accepted a position as co-chair of my combined Ph.D.

Thanks to all of my friends in Mechanical Engineering who started this long journey together. I will never forget the days spent with everyone. I really appreciate seniors and friends in Naval Architecture and Marine Engineering who welcomed me with warm hearts and support when I joined the NAME department. Also, thanks to my good old friends in GLC (Gainax Lover's Club) for their support of all the stress relieving things.

I have been fortunate to have officemates, Jonghun and Ayoung sitting side by side – helping each other, talking or sometimes sharing the virtue of procrastination. Thanks.

Finally, I would like to thank my parents and twin brother for all of the love and support they have given me through my graduate years. Without their encouragement and belief in me, I could not have made this far. Thank you so much.

This research was funded by NDSEG (National Defense Science and Engineering Graduate) fellowship awarded through Department of Defense.

TABLE OF CONTENTS

LIST OF TABLES

Table

LIST OF FIGURES

Figure

LIST OF APPENDICES

NOMENCLATURE

Symbol	Description
$[B_e]$	element strain-nodal displacement matrix
CEER	Cumulative Energy Elimination Rate
$[D_e]$	element constitutive law matrix
DSE	Dynamic Strain Energy
e	e-th redesign variable ($e = 1, \ldots, p$)
E	Young's modulus
E_0	initial Young's modulus
E_e	element Young's modulus
E_s	designer specified (target) Young's modulus
$\{f\}$	force vector
$[k]$	global stiffness matrix
$[k_e]$	element stiffness matrix
$[K]$	generalized stiffness matrix
KE	Kinetic Energy
l	increment number
LEAP	LargE Admissible Perturbations
$[m]$	global mass matrix
$[m_e]$	element mass matrix
$[M]$	generalized mass matrix
n	number of degrees of freedom of structural model
n_a	number of admissibility constraints

$[N_e]$	interpolation function matrix for element
n_r	number of the extracted modal dynamic modes
n_u	number of displacement constraints
n_ω	number of natural frequency constraints
n_d	number of forced response amplitude constraints
n_σ	number of static stress constraints
p	number of redesign variables
RESTRUCT	REdesign of STRUCTures program
s	calculated performance value
s'	performance objective value
S1	baseline (initial) structure
S2	unknown (objective) structure
SSE	Static Strain Energy
$\{u\}$	nodal displacement vector
U_e	equivalent energy level for element

Greek Symbols

α_e	fractional change of redesign variable
Δ	change between state S1 and state S2
$[\Phi]$	dynamic mode shape matrix
$\{\phi\}_i$	i-th dynamic mode shape vector
ω_i^2	i-th modal dynamic eigenvalue

Special Symbols

$(\ )'$	refers to desired structure
$[\ ]^T, \{\ \}^T$	transposed matrix and vector, respectively
$_l(\ )$	refers to l-th increment in the incremental scheme

ABSTRACT

EVOLUTIONARY STRUCTURAL OPTIMIZATION WITH MULTIPLE PERFORMANCE CONSTRAINTS BY LARGE ADMISSIBLE PERTURBATIONS

by

Taemin Earmme

Co-Chairs: Michael M. Bernitsas and Panos Y. Papalambros

A LargE Admissible Perturbation (LEAP) with Evolutionary Structural Optimization methodology is developed. The LEAP methodology uses an incremental predictor-corrector scheme, which makes it possible to solve the redesign problem using data only from the finite element analysis of the baseline structure for changes on the order of 100% in performance and redesign variables without trial and error or repetitive finite element analyses. A structural topology evolution algorithm is introduced using a Cumulative Energy Elimination Rate (CEER) scheme by removing low energy elements at each iteration, while using the elastic modulus in each element as redesign variable in the LEAP methodology. Benchmark examples are used to demonstrate that static displacement, modal dynamic constraints, and simultaneous static and dynamic constraints can be achieved. Convergence is achieved in 3 to 7 iterations with two FEA's per iteration inside the ESO/LEAP algorithm. Results of numerical applications satisfy engineering intuition and show the effect of multiple objectives on topology evolution.

CHAPTER I

INTRODUCTION

A designer knows he has achieved perfection not when there is nothing left to add, but when there is nothing left to take away. (Antoine de Saint-Exupéry)

For decades, the development of Finite Element Analysis (FEA) has played an important role design various and complex structures along with the achievement of computational efficiency. The area of structural optimization has expanded with the advancement of Finite Element Analysis (FEA) in various industry fields from automotive to electronics, mostly designing the mechanical elements and devices. The structural optimization techniques played a major role to obtain a best solution satisfying any engineering specification required by a designer.

Structural optimization can be largely classified into three main areas: size optimization, shape optimization and topology optimization. In size optimization, the goal is to find the optimal thickness distribution of a linearly elastic plate or the optimal member areas in a truss structure. The design domain and the topology of the structure are fixed while changing the size to achieve the design objective. In shape optimization, the boundary of a given topology varies to obtain optimal shape. In a typical case of shape optimization such as the boundary variation method, the objective is to refine the initial shape to an optimized shape, which achieves minimal von Mises equivalent stress in the body.

Topology optimization concentrates on the distribution of material and structural connectivity in the design domain. It aims finding an optimal lay-out of the structure,

which maximizes (or minimizes) an efficiency measure subjected to specific constraints.

The importance of topology optimization is growing to a greater extent recently, since it can provide intuitive concepts to a designer at the early stage of the designing process.

1.1. Literature Review

In Section 1.1.1, the development of general Topology Optimization is reviewed with two major approaches: Homogenization method and Solid Isotropic Material Penalization. Evolutionary Structural Optimization (ESO) related papers are presented in Section 1.1.2 and a development history of LargE Admissible Perturbations (LEAP) methodology is reviewed in Section 1.1.3.

1.1.1. Topology Optimization

Topology optimization is first developed from distributed parameter approaches to shape optimization. Cheng and Olhoff [1] identified that the zero thickness of a plate implies void material in the structure. Their work led to Bendsøe and Kikuchi [2] who first introduced the material distribution for topology design as a computational tool.

Most of topology structural optimization problem frequently studied is the compliance minimization (stiffness maximization) subject to volume constraints. There are two approaches to this problem: the one is the homogenization method and the other is SIMP (Solid Isotropic with Material Penalization) method.

Homogenization Method

In the homogenization method, a homogenized elasticity tensor is formulated to model a unit cell with a rectangular void. (Bendsøe & Kikuchi [2], Bendsøe [3]) The dimensions and orientation angles of the voids are used as the design variables. The initial design domain is homogeneous at the macroscopic scale and the size and orientation of internal rectangular holes are varied to find optimal porosity of the

structure. The method has been successfully applied to solve many types of topology optimization problems (Suzuki [4], Ma & Kikuchi [5], Pederson [6]).

SIMP(Solid Isotropic with Material Penalization) Method

The SIMP (Solid Isotropic with Material Penalization) method is the most widely used minimum compliance formulation. It implements the idea of a penalizing density variable to converge to zero or one, i.e., void or solid (Yang & Chuang [7]). One of the advantages of the SIMP formulation is that it is easy to implement in a Finite Element Analysis framework.

1.1.2. Evolutionary Structural Optimization

Evolutionary Structural Optimization (ESO) was first introduced by Xie and Steven [8] by gradually removing the low stress elements to obtain the objective structure. It has been applied to many individual optimization criteria such as stress, strain, stiffness, natural frequency, buckling, stress minimization, and heat transfer (Chu et al.[9], Zhao, Steven & Xie [10], Manickarajah, Xie & Steven [11], Li et al.[12]) .

The ESO methodology is expanded to Bi-directional Evolutionary Structural Optimization (BESO) (Querin et al.[13], Proos et al.[14], Huang & Xie [15]). The BESO approach allows both removing and adding elements which leads to the optimum more efficiently. BESO methodology was used to design continuum structures with one or multiple materials, or periodic structures utilizing the material interpolation scheme (Huang & Xie [16],[17]).

1.1.3. LargE Admissible Perturbation (LEAP) Methodology

Perturbation based redesign methods have been introduced by Stetson and Palma [18]. They used linear perturbation method to calculate small structural changes necessary which affect the given change in vibration modes. Sandström and Anderson

[19] and Stetson and Harrison [20] developed equations that relate the unknown eigenvectors of the desired structure to the known eigenvectors of the initial structure.

The LargE Admissible Perturbation (LEAP) methodology was first developed to formulate and solve the structural redesign problem. It can solve large scale redesign problems subject to static displacement, natural frequency, forced dynamics amplitude, and static stress constraints. LEAP can achieve changes on the order of 100%-300% without trial and error or repeated finite element analyses. Hoff and Bernitsas [21] introduced static and modal dynamic redesign. The two constraints were integrated in the redesign process by Kim and Bernitsas [22]. Bernitsas and Tawekal [23] solved the model calibration problem by LEAP in a cognate space. Plate and shell elements were added by Bernitsas and Rim [24]. Bernitsas and Suryatama [25] improved the static deflection redesign algorithm by introducing static mode compensation. Bernitsas and Blouin [26] developed a LEAP algorithm to solve the problem of forced response amplitude. The static stress redesign problem was solved by Bernitsas and by Kristanto [27]. Blouin and Bernitsas [28] developed and compared incremental and direct methods for the LEAP algorithm.

The LEAP methodology was first implemented in topology optimization by Suryatama and Bernitsas [29] optimizing a structure which satisfied several performance constraints simultaneously. This was further developed and studied by Miao and Bernitsas [30] and Earmme and Bernitsas [31] using the Evolutionary Structural Optimization method.

1.2. Dissertation Outline

In this dissertation, a structural topology evolution algorithm is developed using LargE Admissible Perturbations (LEAP). The problem formulation for general topology optimization and LargE Admissible Perturbations methodology is described in Chapter II. The general topology optimization is formulated in Section 2.1 and LEAP methodology is presented in Section 2.2.

In Section 2.3, an Evolutionary Structural Optimization scheme is described. The ESO/LEAP algorithm consists of two nested loops. The outer loop is the process of

removal of inefficient elements while the inner loop uses LEAP to find the optimal design which satisfies the performance objectives. The elastic modulus in each element is used as redesign variable in the LEAP methodology. A Cumulative Energy Elimination Rate (*CEER*) scheme is introduced by removing low energy elements, which do not contribute to total performance of the structure, at each iteration.

In Chapter III, the developed methodology is tested by two benchmark examples: cantilever beam and bridge. The numerical results for static displacement, modal dynamic, and simultaneous static displacement and modal dynamic performance constraints are presented from Section 3.1 through Section 3.3. The results for cantilever beam example with increased finite element mesh is exhibited in Section 3.4 and the converged results for varying the value of performance constraints are shown in Section 3.5.

The detailed evolution pattern is further studied in Chapter IV. The evolving topology progress of benchmark example is shown to verify the effectiveness of present methodology. The dissertation contributions/conclusions and suggested future work are summarized in Chapter V.

CHAPTER II

PROBLEM FORMULATION

This Chapter consists of two parts, the first one is the general topology optimization formulation and the second recasts that formulation into a Large Admissible Perturbation form. Those are presented in Sections 2.1 and 2.2, respectively.

2.1. Topology Optimization Formulation

The consistent mass matrix for an isotropic element is

$$[m_e] = \rho_e \int_{V_e} [N_e]^T [N_e] dV \,, \tag{2.1}$$

where ρ_e is the element density, V_e is the element volume, and $[N_e]$ is the interpolation function matrix for each element. Accordingly, the total structural mass matrix can be written as

$$[m] = \sum_{e=1}^{n_e} [m_e] \,. \tag{2.2}$$

Equation (1) shows that by changing the element density, we can change the mass of the structural element.

The stiffness matrix of each element is

$$[k_e] = E_e \int_{V_e} [B_e]^T [D_e][B_e] dV \,, \tag{2.3}$$

where E_e is the elastic Young's modulus, $[D_e]$ is the constitutive law matrix, and $[B_e]$ is the nodal displacement matrix. The stiffness of the element can be changed by modifying E_e.

Let α_e denote the fractional change of ρ_e or E_e. Then,

$$\rho_e' = \rho_e (1 + \alpha_{\rho_e}) \,, \tag{2.4}$$

$$E_e' = E_e (1 + \alpha_{E_e}) \,, \tag{2.5}$$

where α_{ρ_e} and α_{E_e} are the fractional changes of the ρ_e and E_e, respectively. The optimization design variables are all the fractional changes α_e and these small amount of changes are obtained from Large Admissible Perturbation calculations.

Thus, the topology optimization problem can be set as

$$\text{Minimize } \sum_e \alpha_e^2 \,, \tag{2.6}$$

subject to n_u static displacement constraints

$$u_i' = b_{u_i} \qquad i = 1, 2, ..., n_u \,, \tag{2.7}$$

n_ω natural frequency constraints

$$\omega_i'^2 = b_{\omega_i} \qquad i = 1, 2, ..., n_\omega \,, \tag{2.8}$$

n_d forced-response amplitude constraints

$$d_i' = b_{d_i} \qquad i = 1, 2, ..., n_d \,, \tag{2.9}$$

n_σ static stress constraints

$$\sigma_i' = b_{\sigma_i} \qquad i = 1, 2, ..., n_\sigma \,, \tag{2.10}$$

where b_ω, b_u, b_d, and b_σ are the designer performance specifications. Primed quantities refer to the objective structure while unprimed quantities refer to the initial baseline structure. Further, n_a admissibility constraints are imposed from among the complete set

$$\{\phi'\}_j^T [k'] \{\phi'\}_i = 0 \,, \tag{2.11}$$

$$\{\phi'\}_j^T [m'] \{\phi'\}_i = 0 \,, \qquad i = 1, 2, ..., n_\omega \,,\ j = i+1, ..., n_r \,, \tag{2.12}$$

and 2p lower and upper bounds on the redesign variables are imposed

$$-1 < \alpha_e^- \le \alpha_e \le \alpha_e^+ \,,\ \ e = 1, 2, ..., p \,, \tag{2.13}$$

where α_e is element redesign variable, p is the number of redesign variables, α_e^-, α_e^+ are lower and upper bound, respectively. Material specifications on the redesign variables are

$$E_e = 0 \ \text{ or } \ E_s \,. \tag{2.14}$$

The optimization criterion here is the norm of the difference between initial structure and objective structure instead of minimization of compliance which is usually

used in other topology optimization techniques. This allows the designer to obtain a structure that satisfies multiple performance objectives as well as material specifications.

2.2. LargE Admissible Perturbation (LEAP) Formulation

In LEAP methodology, the general perturbation equations are derived by expressing the performance of the unknown (objective) State S2 in terms of baseline (initial) State S1 and the designer's specifications. The static and modal dynamic equations for finite element analysis are written as

$$[k]\{u\} = \{f\}, \tag{2.15}$$

$$([k] - \omega^2[m])\{\phi\} = 0 \tag{2.16}$$

The equations for unknown State S2 are

$$[k']\{u'\} = \{f'\}, \tag{2.17}$$

$$([k'] - \omega'^2[m'])\{\phi'\} = 0. \tag{2.18}$$

Properties of S1 and S2 are related by the perturbation equations (2.19)-(2.22),

$$\text{stiffness matrix} : [k'] = [k] + [\Delta k], \tag{2.19}$$

$$\text{mass matrix} : [m'] = [m] + [\Delta m], \tag{2.20}$$

$$\text{mode shape} : \{\phi'\} = \{\phi\} + \{\Delta\phi\}, \tag{2.21}$$

$$\text{displacement} : \{u'\} = \{u\} + \{\Delta u\}, \tag{2.22}$$

where Δ represents the difference between State S1 and State S2. Substituting (2.19), (2.20) and (2.22) into (2.17) and (2.18) yields

$$\{\Delta u\} = -\{u\} + ([k] + [\Delta k])^{-1}\{f'\}, \tag{2.23}$$

$$\{\phi'\}^T([\Delta k] - \omega'^2[\Delta m])\{\phi'\} = -\{\phi'\}^T([k'] - \omega'^2[m'])\{\phi'\}. \tag{2.24}$$

where $[\Delta k]$ and $[\Delta m]$ are functions of redesign variables α_e. For rod and beam elements, the stiffness and mass matrices depend linearly on α_e. However, in the case of plate elements, the stiffness matrix for bending is a cubic form [24]. We use eight node solid elements, CHEXA elements in MSC/NASTRAN for all the numerical analysis in this work.

$$[\Delta k] = \sum_{e=1}^{p}[\Delta k_e] = \sum_{e=1}^{p}[k_e]\alpha_e, \tag{2.25}$$

$$[\Delta m] = \sum_{e=1}^{p}[\Delta m_e] = \sum_{e=1}^{p}[m_e]\alpha_e. \tag{2.26}$$

Substituting (2.25) into (2.23), we derive the static general perturbation. (See Appendix A) Additionally, substituting (2.19)-(2.22) and (2.25)-(2.26) into (2.24), we get the general perturbation equation for modal dynamics.

The static general perturbation equation can be written as

$$u_i' = u_i - \sum_{m=1}^{n_r}\phi_{i,m}'\frac{\sum_{e=1}^{p}\{\phi'\}_m^T[k_e]\{u\}\alpha_e}{\{\phi'\}_m^T[k]\{\phi'\}_m + \sum_{e=1}^{p}(\{\phi'\}_m^T[k_e]\{\phi'\}_m)\alpha_e}, \text{ for } i, j = 1, 2, ..., n \tag{2.27}$$

Also the general perturbation equation for modal dynamics can be shown as

$$\sum_{e=1}^{p}(\{\phi'\}_j^T[k_e]\{\phi'\}_i - \omega_i'^2\{\phi'\}_j^T[m_e]\{\phi'\}_i^T)\alpha_e = \omega_i'^2\{\phi'\}_j^T[m]\{\phi'\}_i - \{\phi'\}_j^T[k_e]\{\phi'\}_i$$

for $i, j = 1, 2, ..., n$ (2.28)

Detailed derivation for (2.28) is shown in Appendix B.

For the general perturbation equation for forced response amplitudes and static stresses, refer to Bernitsas and Blouin [26] and Bernitsas and Kristanto [27], respectively. The general perturbation equations (2.27) and (2.28) are implicit nonlinear equations with respect to α_e which cannot be solved directly. Thus, we have developed an incremental predictor and a corrector scheme to optimize these equations. This concept is outlined in Figure 2.1.

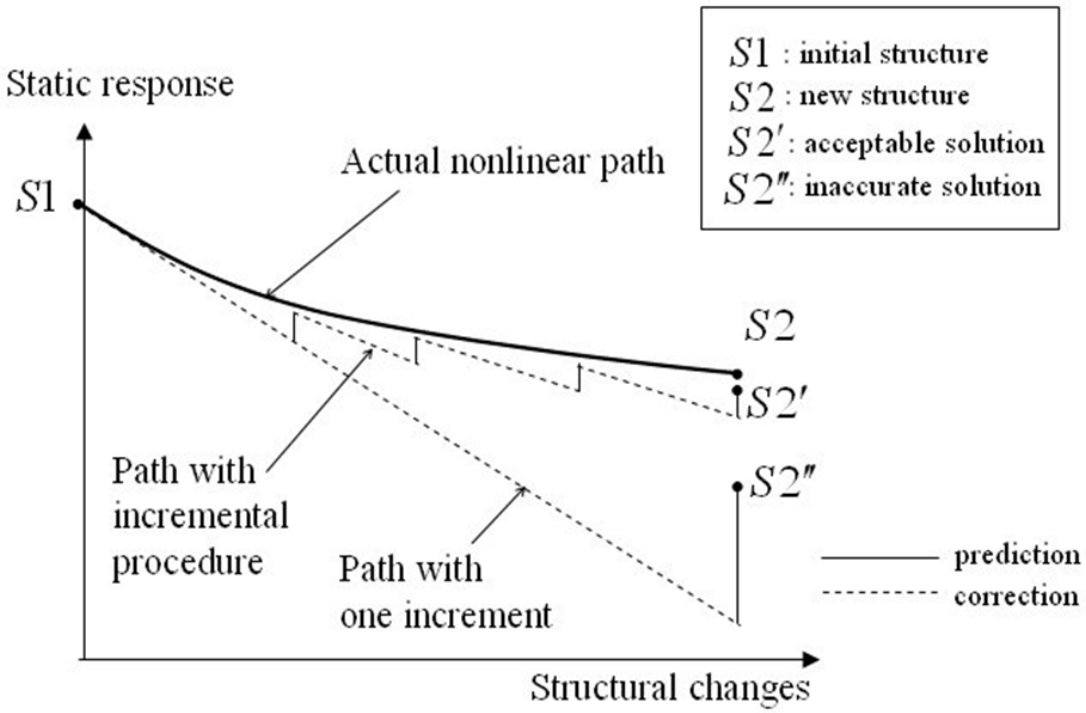

Figure 2.1 Schematic representation of solution process

To illustrate the incremental predictor and corrector scheme, we use the static redesign problem below. The desired change in static response is divided into N small increments. Subscript l denotes the number of each increment.

Considering the optimization problem defined in (2.6)-(2.13), the incremental redesign problem can be written as

$$\text{Minimize } \sum_{e=1}^{p}[(1+\alpha_e^l)\prod_{q=1}^{l-1}(1+\alpha_e^q)-1]^2, \tag{2.29}$$

subject to

$$u_i'^l = b_{u_i}^l \qquad i=1,2,...,n_u, \tag{2.30}$$

$$\omega_i'^{2^l} = b_{\omega_i}^l \qquad i=1,2,...,n_\omega, \tag{2.31}$$

$$d_i'^l = b_{d_i}^l \qquad i=1,2,...,n_d, \tag{2.32}$$

$$\sigma_i'^l = b_{\sigma_i}^l \qquad i=1,2,...,n_\sigma, \tag{2.33}$$

$$\{\phi'\}_j^{T^l}[k'^l]\{\phi'\}_i^l = 0 \tag{2.34}$$

$$\{\phi'\}_j^{T^l}[m'^l]\{\phi'\}_i^l = 0, \tag{2.35}$$

$$\text{for } \; i=1,2,...,n_\omega, \; j=i+1,...,n_r,$$

and the lower and upper bounds are

$$0 < \frac{1+\alpha_e^-}{\prod_{q=1}^{l-1}(1+\alpha_e^q)} \le 1+\alpha_e^l \le \frac{1+\alpha_e^+}{\prod_{q=1}^{l-1}(1+\alpha_e^q)}, \tag{2.36}$$

where $\prod_{q=1}^{l-1}(1+\alpha_e^q)$ is known from all previous increments. For the first iteration, *l* is equal to 1 by definition.

While selecting the optimal criterion as to equal the end of incremental change to completion of the solution process, criterion (2.6) is satisfied since

$$1+\alpha_e = \prod_{q=1}^{N}(1+\alpha_e^q) \tag{2.37}$$

At the same time, the performance constraints satisfy the general perturbation equation such as (2.27) and (2.28).

At each increment, equations (2.29)-(2.35) need to be solved to obtain the unknown fractional changes $\alpha_e^l, e=1,...p$, The eigenvectors $\{\phi'\}_m^l, m=1,...,n_r$ in general perturbation equation (2.27) are approximated by the known eigenvectors $\{\phi\}_m$ of the initial structure in the first increment. For subsequent increments in the prediction phase, the eigenvectors are approximated by the ones which are computed in the previous increments. The optimization problem is solved to obtain the incremental fractional changes which predict the solution. From this, the eigenvectors are updated (see Appendix C). With new updated eigenvectors, corrector scheme is conducted to obtain the fractional changes $\alpha_e^l, e=1,...p$. A schematic representation of this algorithm is depicted in Figure 2.2.

The LEAP methodology is currently implemented by FORTRAN 77 language. It is named as RESTRUCT (REdesign of STRUCTures) and uses MSC/NASTRAN database and user defined files as input files. For the nonlinear optimization, Feasible Sequential Quadratic Programming (FSQP) algorithm is used which was developed by the Institute for Systems Research (ISR), University of Maryland. The key features of FSQP related to the present work are described in Appendix D.

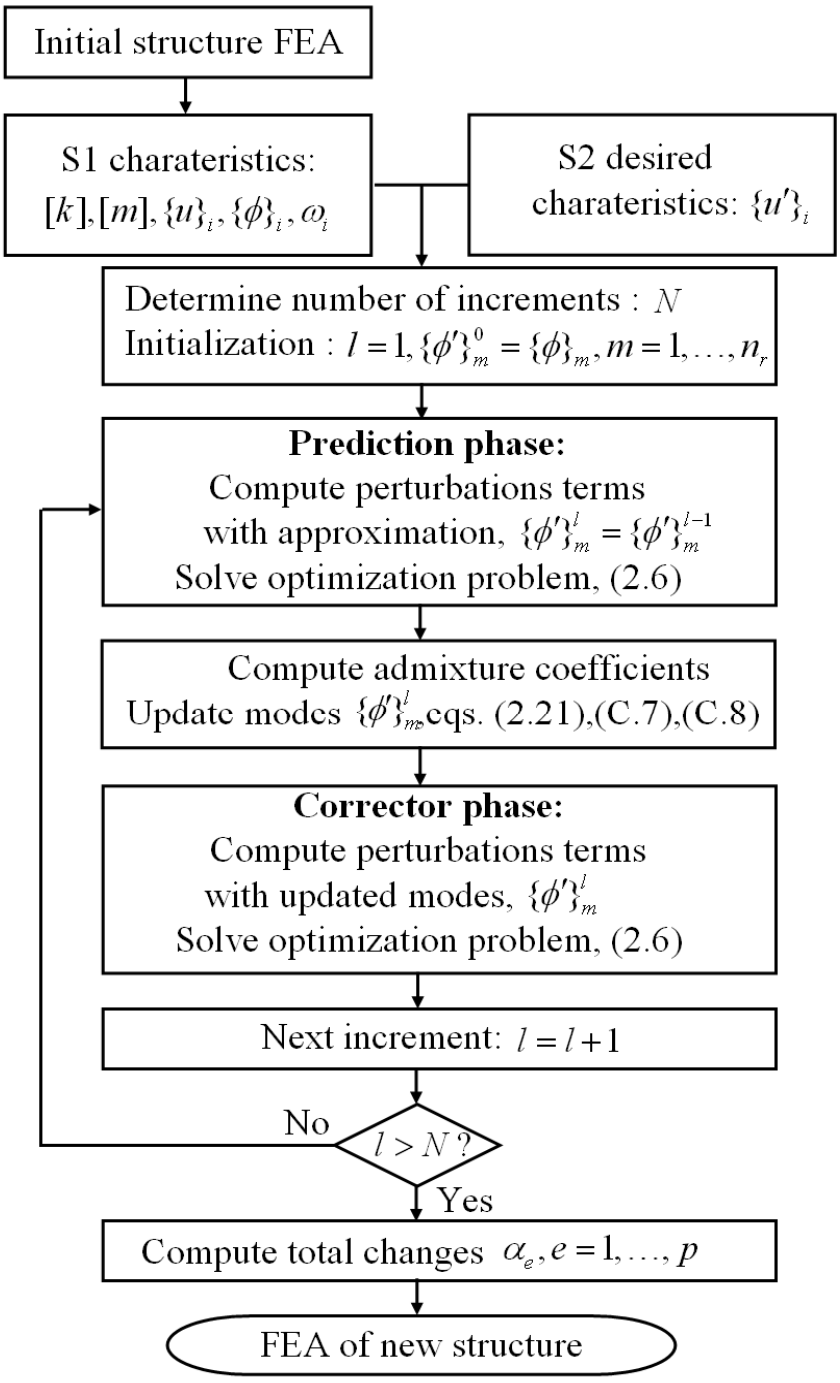

Figure 2.2 Algorithmic Representation of Incremental Method

2.3. Evolutionary Structural Optimization (ESO) Algorithm

The ESO algorithm developed in this work consists of two nested loops. The inner loop, which uses LEAP to calculate the performance equations into a form that can be handled without trial and error or repeated FEA's, finds incrementally the optimal design which satisfies the objectives. The outer loop implements the search for the optimal topology. The major characteristics of the ESO/LEAP algorithm developed in this work are the following:

(1) The optimal topology is achieved in 3-7 iterations. In each iteration, the starting (baseline) topology has been generated in the previous iteration. The initial topology is a uniform, homogeneous, solid block.
(2) In the inner loop of each iteration, the LEAP algorithm is used to optimize the structure generated by the outer loop to achieve the redesign objectives and calculate the optimization variables α_e.
(3) Following the LEAP optimization within each iteration, two heuristic criteria are used to modify the topology in a rational way. Both address the extremes of the stiffness of the generated elements. The first criterion eliminates elements at the lower end of the stiffness values. The second criterion replaces high stiffness elements by the upper limit of stiffness, which is equal to the stiffness of the available material.

In Sections 2.3.1 through 2.3.3, the heuristic criteria implemented in the topology evolution process are presented, while in Section 2.4, the major steps of the ESO/LEAP algorithm are described.

2.3.1. Element Elimination Criterion

To eliminate the inefficient elements, which do not contribute to the total performance of the structure, a rejection criterion is employed. For static topology design, the material efficiency can be measured by Static Strain Energy (SSE). Gradual removal

of the lower static strain energy elements leads to a more uniform distribution of material efficiency in the evolving optimal topology compared to the initial structure. For dynamic modal redesign, the material efficiency is measured by both the Dynamic Strain Energy (DSE) and the Kinetic Energy (KE). Accordingly, the rejection criterion places a lower limit on a predefined expression of the material efficiency that includes both DSE and KE. Theoretically, the total DSE of the structure is equal to the total KE in free vibration. The distribution of DSE, however, is different from that of KE, that is, DSE and KE are not the same for individual elements. Thus, we need to consider both DSE and KE in the material efficiency measure.

Consequently, an equivalent energy level U_e can be defined as a material efficiency measure as follows. For static displacement constraints,

$$U_e = SSE\,, \tag{2.38}$$

for modal dynamic constraints,

$$U_e = w_1 \times DSE + w_2 \times KE\,, \tag{2.39}$$

for simultaneous static and dynamic constraints,

$$U_e = w_1 \times DSE + w_2 \times KE + w_3 \times SSE\,, \tag{2.40}$$

where w_1, w_2 and w_3 are the weight factors for DSE, KE and SSE respectively. For modal dynamics topology design, w_1 and w_2 are both set equal to 0.5. For simultaneous static and modal dynamics topology design, w_1, w_2 and w_3 are set equal to 0.25, 0.25 and 0.5, respectively. It should be noted that all three energies – DSE, KE, and SSE – are normalized individually to 1. To normalize these energies, each element's energy is simply divided by the total amount of element energy.

To eliminate the low energy level elements, first the equivalent energy level U_e for each element is calculated. At the same time, the energy level U_{total} for the total

elements in the structure is computed. All elements that satisfy the following criterion are rejected.

$$\frac{U_e}{U_{total}} < CEER\,. \tag{2.41}$$

If the element is removed, its Young's modulus is set to a very low value close to zero (weak material) to represent the element elimination. The elements removed virtually do not carry any load and their energy levels are negligible. The advantage of this method is that it does not need to regenerate a new finite element mesh at each iteration even if the developed structure largely differs from initial structure.

Determining the value of the Cumulative Element Elimination Rate (*CEER*) is explained in the next section.

2.3.2. Cumulative Energy Elimination Rate (CEER)

The Cumulative Energy Elimination Rate (*CEER*) is defined as the sum of energy of the low energy elements, which are removed at each iteration, over the sum of energy in all elements.

$$CEER = \begin{cases} CEER_{initial} \times \dfrac{U^i_{\max}}{U^{i-1}_{\max}} & (if \quad U^i_{\max} \le U^{i-1}_{\max}) \\ CEER_{\min} & (otherwise) \end{cases} \tag{2.42}$$

where $CEER_{initial}$ is a predefined parameter and $U^{i-1}_{\max}$ and $U^i_{\max}$ are the maximum element energy in $(i-1)$th and ith iteration, respectively. $CEER_{\min}$ is a predefined minimum elimination rate. The energy elimination rate is recalculated by multiplying the ratio of current maximum energy to previous maximum energy of an element. As topology evolves, *CEER* needs to be decreased to eliminate fewer elements otherwise it may remove useful (contributing) elements. If a fixed rate elimination scheme is applied, convergence is not always achieved because there is a possibility that it might remove the useful elements making the structure disconnected. In case the maximum energy of

current iteration exceeds the previous iteration, we assign the *CEER* a minimum elimination rate, which is a very small value between 0.001 and 0.015. At this stage, minimum elimination rate should be applied since every remaining element carries concentrated energy. Under this condition, the total energy distribution is approaching convergence level and therefore $CEER_{\min}$ should be used.

2.3.3. Element Freezing Criterion

Following elimination of the low efficiency elements based on the *CEER* criterion, the element freezing criterion is used to manage the other extreme of Young's modulus. Specifically, elements with values of Young's modulus greater than E_s are assigned a value of Young's modulus equal to E_s, which is defined by the designer. This process, on one hand, makes the material more uniform and on the other hand, places an upper limit on the extreme values of Young's modulus generated in the redesign process. Accordingly, the optimal material distribution produced by RESTRUCT is adjusted based on the following criterion

$$E_e^{i+1} = \begin{cases} E_s, & E_e^i \geq E_s \\ E_e^i, & E_e^i < E_s \end{cases} \tag{2.43}$$

where E_e^{i+1} is the Young's modulus of element e for the next iteration. E_e^i is the current element material property in RESTRUCT. When the material property of an element reaches E_s, it is frozen at the material value of E_s In the rest of the optimization process, only the elements that have not been eliminated or have not been frozen are used.

2.4. Optimization Process Steps

There are two loops in the optimization process. The outer loop sets the updated topology based on the two heuristic criteria defined above. The inner loop optimizes the

redesign variables to achieve the performance objectives. The major steps of the ESO/LEAP algorithm are shown schematically in Figure 2.3.

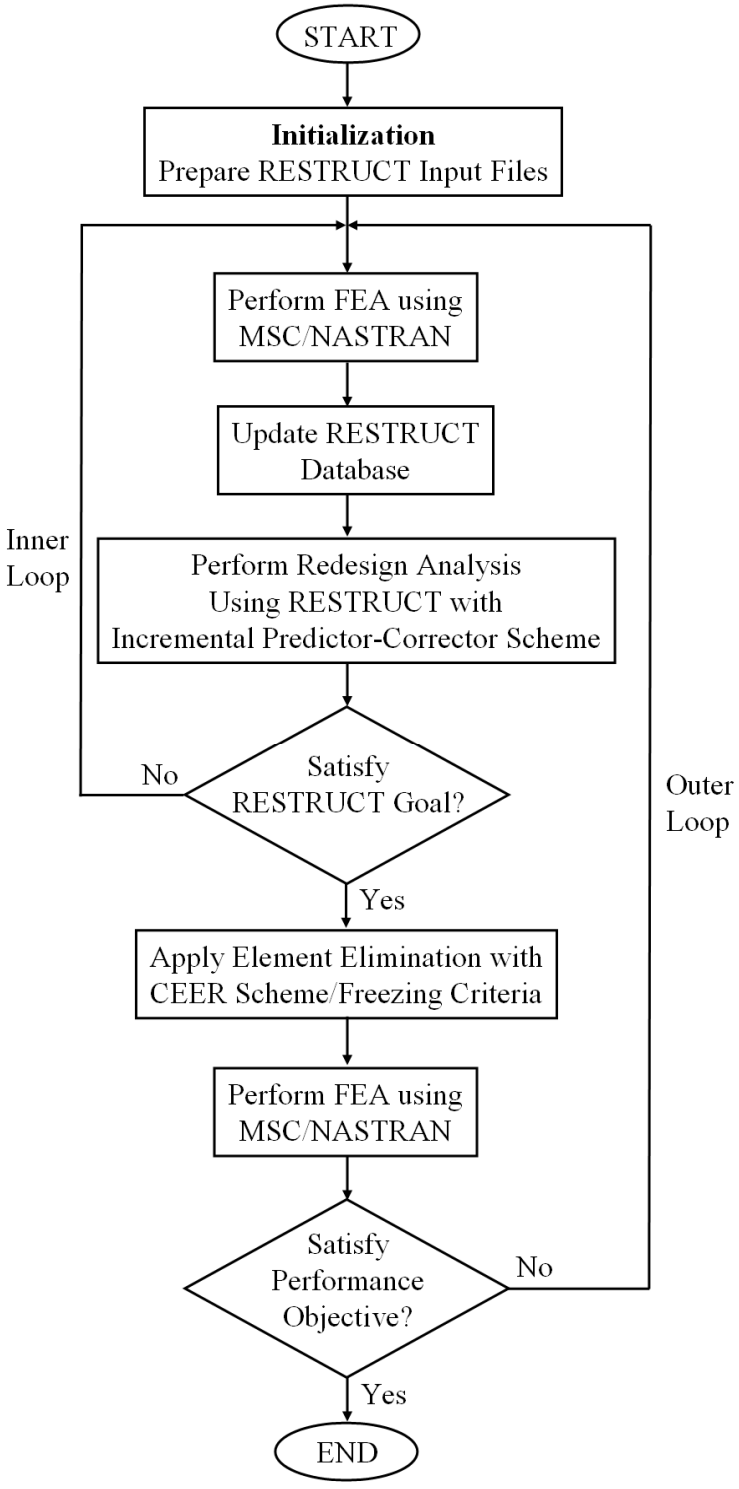

Figure 2.3 Algorithmic Representation of ESO/LEAP
(Evolutionary Structural Optimization / LargE Admissible Perturbation) methodology

For the inner loop, RESTRUCT process is used to find the structural changes, α_e by incremental predictor-corrector scheme which is explained in Section 2.2. If the calculated results satisfy the performance goals, it continues to the next step. The element elimination is applied with Cumulative Energy Elimination Rate (*CEER*) and freezing criteria. Then Young's modulus values of all elements which are not eliminated and Young's modulus value is below E_s, are set to E_s temporarily. This process is to check whether the structure with Young's modulus properties of the elements are all equal to E_s satisfies the performance criteria or not. If it satisfies the criteria, stop the optimization process and converged result is obtained.

The optimization criteria for the outer loop are the norm between desired performance objective and calculated performance values. It can be written as

$$\left|s' - s\right| < \varepsilon \tag{2.44}$$

where s' is designer specified performance objectives and s is calculated performance values. If the absolute value of difference is less than ε, optimization process is terminated and we get a new objective structure. 5% is used as the criteria value for this work. If the criterion is not satisfied, it returns to the beginning of the RESTRUCT process as depicted in Figure 2.3.

CHAPTER III

PARAMETRIC EVOLUTION RESULTS

In this Chapter, two numerical applications are presented in static, dynamic, and simultaneous (static and dynamic) redesign. The first application is a cantilever beam with a concentrated force applied at the free-end as shown in Figure 3.1. The design domain has length 16 mm, height 10 mm and thickness 3 mm. Initial Young's modulus is $E_0 = 2.07 \times 10^5 MPa$, Poisson's ratio $\nu = 0.3$, and mass density $\rho = 7.833 \times 10^{-9} Ns^2 / mm^4$. A 300N force is applied downward at the center of the free-end. A finite element mesh of 32×20 is used.

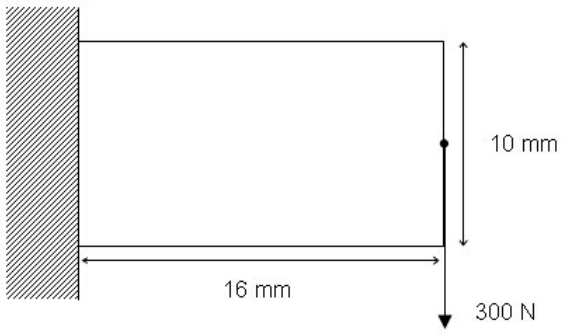

Figure 3.1. Cantilever beam with one point load at the center of the free-end

The second example is a simply supported bridge with three point forces [5]. Loads are applied to the bottom of the initial structure. It has a 60 mm $\times$ 20 mm domain with 1 mm thickness. Initial Young's modulus $E_0 = 2.07 \times 10^5 MPa$, Poisson's ratio $\nu = 0.3$, and

mass density $\rho = 7.833 \times 10^{-9} Ns^2 / mm^4$. The design domain is discretized using a 36×12 grid; that is, a total of 432 finite elements.

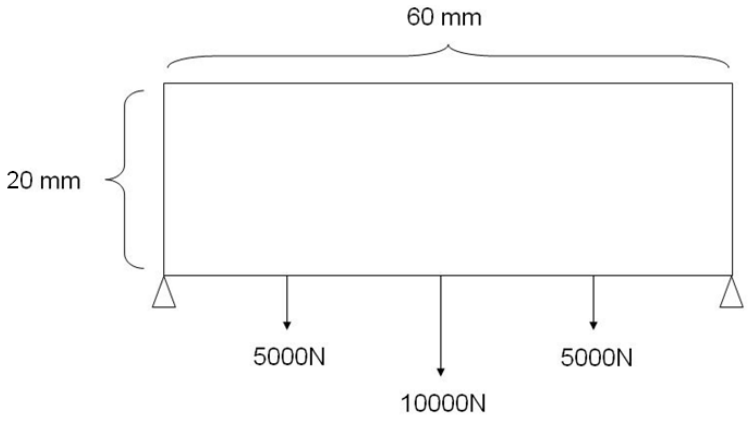

Figure 3.2. Bridge with three point loads

The structural performance specifications of the cantilever beam and bridge for static displacement, modal dynamic, and simultaneous static displacement and modal dynamic constraints are shown in Table 3.1 and 3.2, respectively. For example, $u'/u = 0.5$ means decreasing static displacement by half of the initial displacement. ω'^2/ω^2 denotes the ratio between the initial and target eigenvalues. Note that for modal dynamic performance constraints, the first in-plane mode is considered. $CEER_i$ represents the varying values of Cumulative Energy Elimination Rate (*CEER*) at *i*-th iteration.

The initial Young's modulus E_0 is set equal to 1.0 while the designer specified target Young's modulus E_s is varied from 2.0 to 3.5 depending on the specific examples. It is noteworthy to mention that previous ESO methods use material density ρ to 0 or 1 as design variable [15,16]. This means that the Young modulus is not varied and its initial value is used as a fixed value. The ESO using the LEAP methodology developed in this work allows to change Young's modulus to achieve better structural performance simultaneously eliminating mass as needed.

Table 3.1. Structural performance specifications for cantilever beam application

Objective		*Stiffness*	
		$E_s = 3.0$	$E_s = 3.5$
Static :	$\frac{u'}{u} = 0.5$	$^{*}CEER_i = 0.05, 0.015,$ $0.015, 0.015, 0.015$	$CEER_i = 0.05, 0.015,$ 0.015
Dynamic :	$\frac{\omega'^2}{\omega^2} = 1.44$	$CEER_i = 0.05, 0.020,$ $0.010, 0.010, 0.010$	$CEER_i = 0.05, 0.031,$ $0.038, 0.015, 0.015,$ $0, 015$
Static & Dynamic :	$\frac{u'}{u} = 0.65$ $\frac{\omega'^2}{\omega^2} = 1.44$	$CEER_i = 0.05, 0.032,$ $0.045, 0.0025, 0.0025,$ 0.0025	$CEER_i = 0.045, 0.038,$ $0.044, 0.015, 0.015,$ 0.015

* $CEER_i$ values evolving from the algorithm during the topology evolution process at each iteration ($i = 1, 2, \ldots$)

Table 3.2. Structural performance specifications for bridge application

Objective		*Stiffness*	
		$E_s = 3.0$	$E_s = 3.5$
Static :	$\frac{u'}{u} = 0.5$	$^{*}CEER_i = 0.05, 0.029,$ $0.041, 0.015$	$CEER_i = 0.05, 0.033,$ $0.042, 0.015, 0.015$
Dynamic :	$\frac{\omega'^2}{\omega^2} = 2.0$	$CEER_i = 0.03, 0.026,$ $0.022, 0.009$	$CEER_i = 0.04, 0.036,$ $0.012, 0.012$
		$E_s = 2.0$	$E_s = 2.5$
Static & Dynamic :	$\frac{u'}{u} = 0.6$ $\frac{\omega'^2}{\omega^2} = 1.8$	$CEER_i = 0.04, 0.019,$ $0.012, 0.012$	$CEER_i = 0.04, 0.023,$ $0.038, 0.012, 0.012,$ $0.012, 0.012$

* $CEER_i$ values evolving from the algorithm during the topology evolution process at each iteration ($i = 1, 2, \ldots$)

3.1. Static Displacement Problem

As shown in Table 3.1 and Table 3.2, the static displacement objective is to decrease the displacement at the loading point by a factor of 2. It is tested using two target values for E_s, 3.0 and 3.5. That is, the element Young's modulus starts from initial value E_0=1.0 and increased up to the target E_s value of 3.0 or 3.5. The initial *CEER* value is set at 0.05.

3.1.1. Cantilever Beam

For the cantilever beam problem, the results of target Young's modulus 3.0 and 3.5 are summarized in Figure 3.3 and Figure 3.4, respectively. We can make the following observations based on these results:

(a) The resulting topology exhibits a Gothic arch-like form.
(b) There is a clear pattern in mass voids with hinges appearing along the horizontal axis of symmetry of the structure.
(c) As expected, the mass of the structure decreases with increasing stiffness; that is, higher E_s. Obviously, less material is required to satisfy the static displacement objective when we use stiffer material.

The number of iterations required for convergence and the volume reduction percentage for the static cantilever beam problem are shown in Table 3.3.

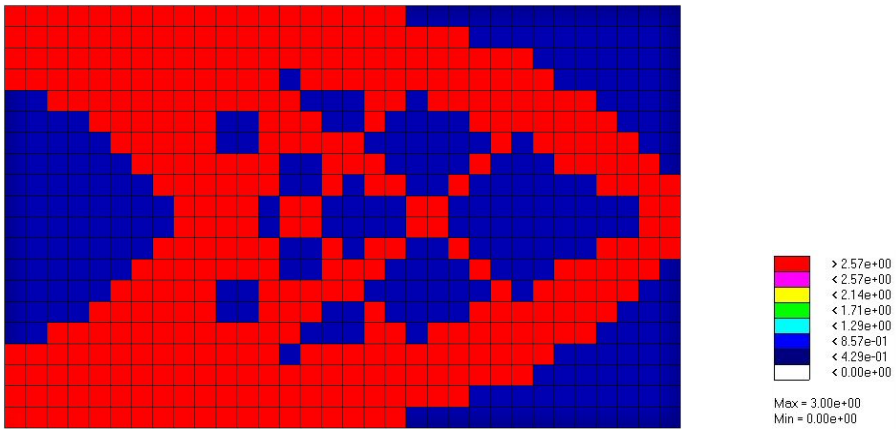

Figure 3.3. Evolved cantilever beam for static displacement objective and $E_s = 3.0$

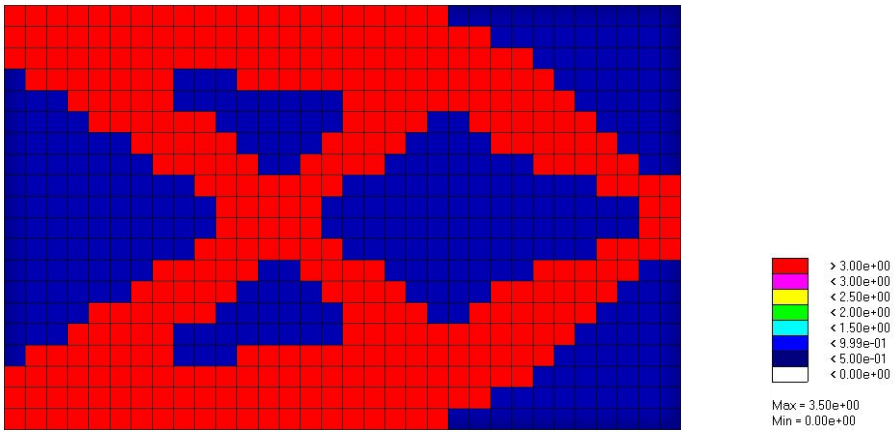

Figure 3.4. Evolved cantilever beam for static displacement objective and $E_s = 3.5$

Table 3.3. Number of iterations and volume reduction percentage for static cantilever beam evolution

Stiffness	*Number of iterations*	*Volume reduction percentage*
$E_s = 3.0$	5	41.9%
$E_s = 3.5$	3	46.9%

Comparing present work to the recently developed Bi-directional Evolutionary Structural Optimization (BESO) method, the ESO/LEAP achieves very similar topology only in three iterations while the BESO methodology requires at least 70 iterations [15]. Further, the BESO method, when the volume reaches its objective value, which is 50% of the total design domain, the mean compliance converges to a constant value of 1.87 Nmm. The present method achieves volume reduction of 46.9% and mean compliance of 1.60 Nmm with significantly decreased number of iterations.

3.1.2. Bridge

The objective of the bridge example is to reduce static displacement by half at mid-span of the bridge bottom, where the largest force is applied. The converged results are shown in Figure 3.5 and Figure 3.6 using two different E_s values of 3.0 and 3.5, respectively. The number of iterations and volume reduction percentages are listed in Table 3.4. The resulting topology exhibits the following features:

(a) Curved and straight elements evolved from the initial solid structure to form a bridge-like structure to support the three point loads while observing the two fixed boundary points.
(b) Using higher E_s, i.e., stiffer material, requires less material to achieve the specified performance.
(c) There is similarity in voids and joints between the two cases. In the less stiff material case, more material is required to support the applied loads. As expected, the higher Young's modulus structure develops thinner members than the less stiff material case.
(d) The lack of bridge bottom can be justified intuitively. Loads are not applied along the entire bottom of the bridge. Accordingly, the three vertical structural members evolve which transfer the bottom loads to the arch above which is a most efficient way of supporting loads between two boundaries.

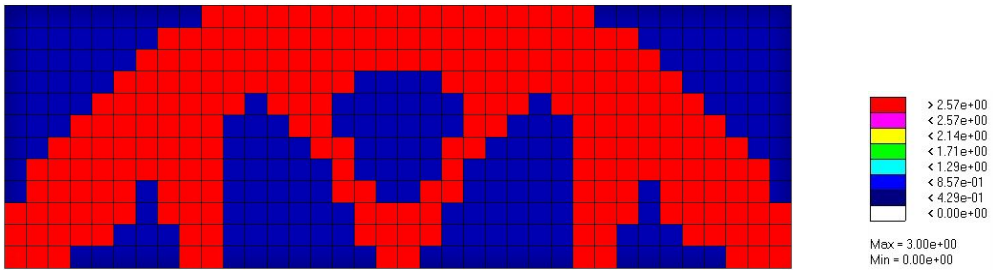

Figure 3.5. Evolved bridge for static displacement objective and $E_s = 3.0$

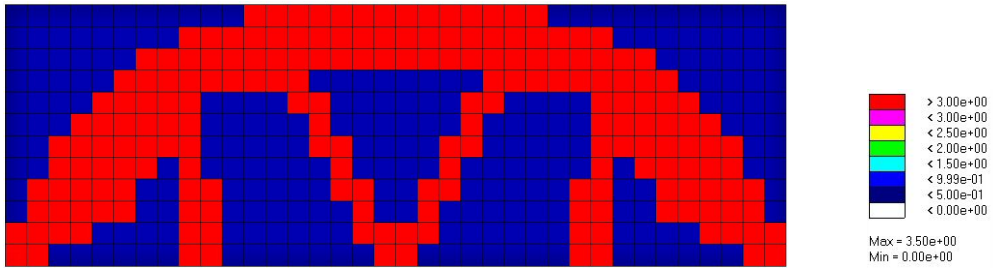

Figure 3.6. Evolved bridge for static displacement objective and $E_s = 3.5$

Table 3.4. Number of iterations and volume reduction percentage for static bridge evolution

Stiffness	*Number of iterations*	*Volume reduction percentage*
$E_s = 3.0$	4	45.4%
$E_s = 3.5$	5	54.6%

3.2. Modal Dynamic Problem

The modal dynamic problem is to increase the first eigenvalue corresponding to the in-plane bending mode. For the cantilever beam, the objective is to increase the first eigenvalue by a factor of 1.44. For the bridge, the objective is to increase the first eigenvalue by a factor of 2.0.

3.2.1. Cantilever Beam

Figure 3.7 and Figure 3.8 show the evolved structure for the modal dynamic requirement for target Young's modulus of E_s =3.0 and 3.5, respectively. The number of iterations and volume reduction percentages are tabulated in Table 3.5. Similar topological characteristics evolve in both cases while intuitively reasonable differences appear.

(a) Material is lumped near the free-end providing the mass needed to achieve the new higher frequency while voids appear close to the clamped end. This can be intuitively justified since when mass is shifted towards to clamped end of the beam, effectively extending the clamped end leaving a shorter free-end for oscillation.
(b) Using higher E_s value, results in less material needed to satisfy the performance constraints. Similar topological features evolve with additional voids in the higher E_s case.

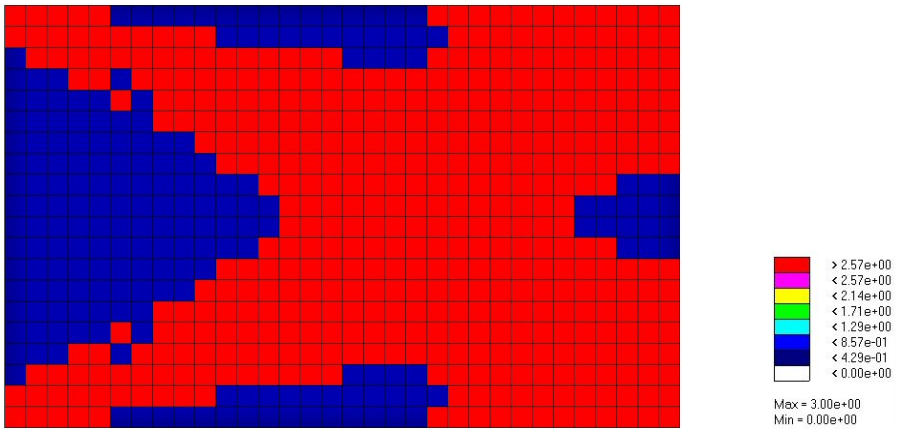

Figure 3.7. Evolved cantilever beam for modal dynamic objective and $E_s = 3.0$

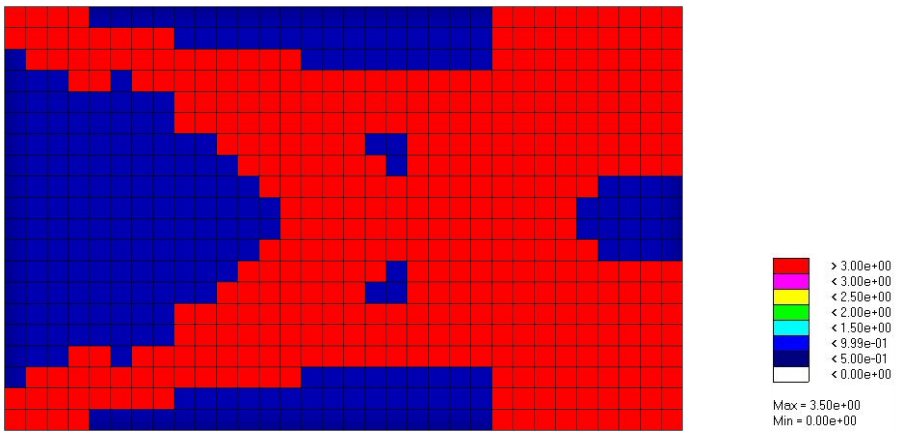

Figure 3.8. Evolved cantilever beam for modal dynamic objective and $E_s = 3.5$

Table 3.5. Number of iterations and volume reduction percentage for modal dynamic cantilever beam evolution

Stiffness	*Number of iterations*	*Volume reduction percentage*
$E_s = 3.0$	5	31.3%
$E_s = 3.5$	6	38.1%

3.2.2. Bridge

For the bridge topology evolution examples, the modal dynamic performance objective is to increase the first eigenvalue of the in-plane bending mode by a factor of 2.0. The results are shown in Figure 3.9 and Figure 3.10. using E_s =3.0 and 3.5, respectively. The following observations can be made:

(a) For both cases, the mass is preserved in the middle of the structure where the amplitude of oscillation is higher.
(b) Higher target Young's modulus E_s results in voids near the end supports – away from the high oscillations at the center of the bridge. This decreases the total volume. The modal dynamic requirement is still satisfied in spite of the reduced stiffness. The higher E_s compensates for loss of stiffness.

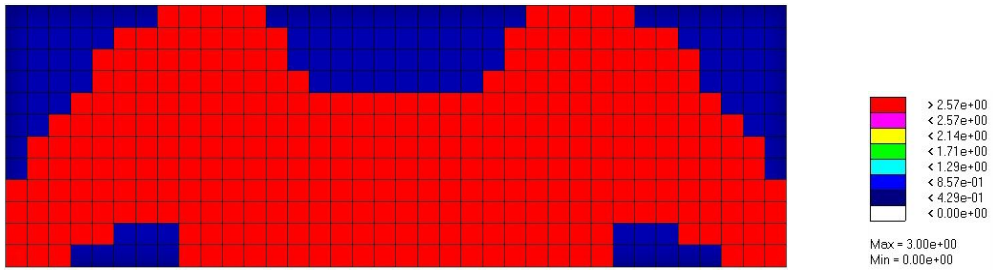

Figure 3.9 Evolved bridge for modal dynamic objective and $E_s = 3.0$

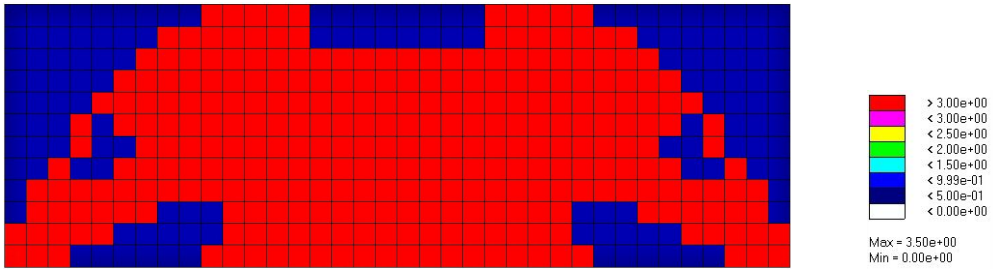

Figure 3.10 Evolved bridge for modal dynamic objective and $E_s = 3.5$

Table 3.6. Number of iterations and volume reduction percentage for modal dynamic bridge evolution

Stiffness	*Number of iterations*	*Volume reduction percentage*
$E_s = 3.0$	4	25.4%
$E_s = 3.5$	4	31.5%

3.3. Simultaneous Static and Modal Dynamic Problem

In this section, static displacement and modal dynamic performance objectives are considered at the same time. As shown in Table 3.1, the objectives for the cantilever beam topology evolution are to reduce the displacement of a specific point by a factor of 0.65 for the cantilever beam and to increase the first eigenvalue of the in-plane bending mode by a factor of 1.44. For the bridge example, the objective for static displacement is to reduce the amplitude by a factor of 0.6 and simultaneously to increase the first eigenvalue by a factor of 1.8. The initial Cumulative Energy Elimination Rate (*CEER*) is 0.045 for cantilever beam and 0.04 for the bridge example.

3.3.1. Cantilever Beam

Two different target values for Young's modulus are tested, E_s =3.0 and 3.5. The results are presented in Figure 3.11 and Figure 3.12, respectively. In these results, we can easily find coexisting features which appeared in the single objective examples. For the E_s =3.0 case, the mass is shifted from the middle to the free-end part while the clamped end still maintains the topological features from the static displacement results. In the case of E_s =3.5, the structure more looks like combined topology of static and modal dynamic examples. It still retains the Gothic-arch form in the middle of the structure while the mass is distributed more to the free-end to achieve the dynamic performance objective. Note that these results are obtained in only 6 or 7 iterations as shown in Table 3.7.

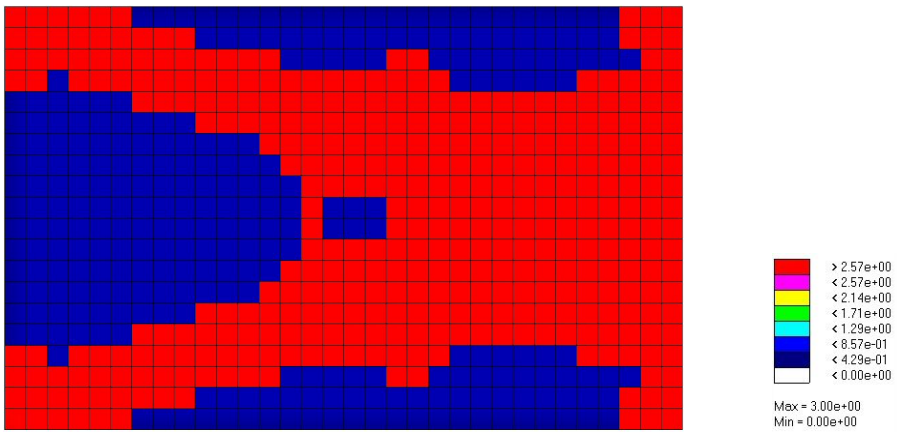

Figure 3.11. Evolved cantilever beam for static displacement/modal dynamic objective and $E_s = 3.0$

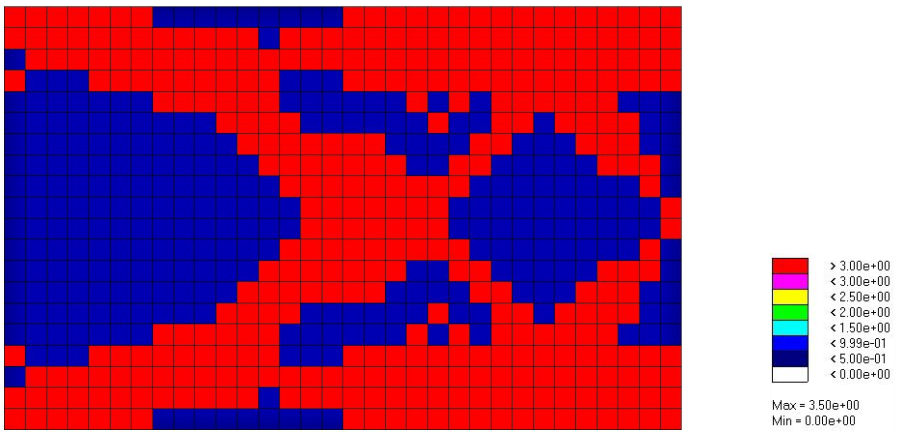

Figure 3.12. Evolved cantilever beam for static displacement/modal dynamic objective and $E_s = 3.5$

Table 3.7. Number of iterations and volume reduction percentage for static displacement and modal dynamic of cantilever beam evolution

Stiffness	*Number of iterations*	*Volume reduction percentage*
$E_s = 3.0$	6	42.5%
$E_s = 3.5$	7	44.4%

3.3.2. Bridge

In this example, target Young's modulus values of E_s =2.0 and 2.5 are used. The converged results are shown in Figure 3.13 and Figure 3.14. These results show simultaneous characteristics observed in the static displacement and modal dynamic cases independently. The following observations are made:

(a) The overall arch shape which evolved in the static displacement case is still predominant.
(b) Mass is lumped near the center where maximum oscillation occurs.
(c) The three voids observed in the static displacement evolution are still present in the middle. The size of the voids, however, is decreased.

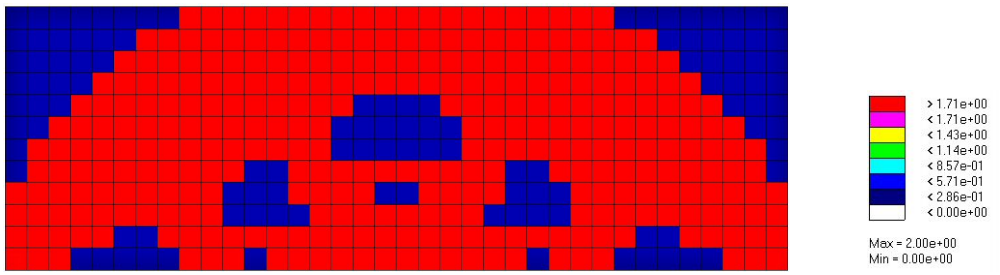

Figure 3.13. Evolved bridge for static displacement/modal dynamic objective and $E_s = 2.0$

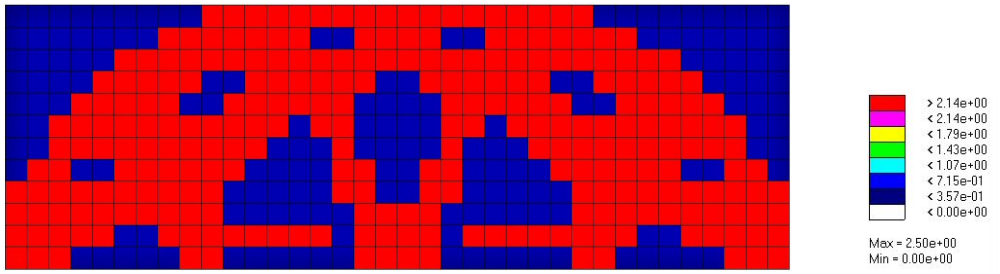

Figure 3.14. Evolved bridge for static displacement/modal dynamic objective and $E_s = 2.5$

Table 3.8. Number of iterations and volume reduction percentage for static displacement and modal dynamic bridge evolution

Stiffness	*Number of iterations*	*Volume reduction percentage*
$E_s = 2.0$	4	25.9%
$E_s = 2.5$	6	38.4%

The advantage of applying the Cumulative Energy Elimination Rate (*CEER*) scheme instead of fixed rate elimination method [30], the converged result is obtained much faster. For example, it requires 6 or 10 iterations to get the similar converging results in static problem $E_s = 3.5$ while it takes only 3 iterations. All the other examples in the present work show less or same number of iterations.

Additionally, since fixed elimination rate method removes constant number of elements at each iteration, it sometimes eliminates useful elements which are critical to structural stability. The *CEER* scheme can overcome this problem by removing very small portion of the elements when the optimization process is close to convergence.

3.4. Topology Evolution with Increased Resolution

In this section, the cantilever example with increased resolution of the finite element mesh is tested. A finite element mesh of 48×30 is used. The performance constraints applied are same as shown in Table 3.1. Only the static displacement and modal dynamic constraints are applied separately. The designer specified target Young's modulus E_s is set equal to 3.0.

Evolved cantilever beam for static displacement and modal dynamic objective are exhibited in Figure 3.15 and Figure 3.16, respectively. Comparing these results to the 32×20 mesh results, which are shown in Figure 3.3 and Figure 3.7, very similar characteristics can be observed. The topological features are similar in both applications with nearly the same volume reduction achieved. As shown in Table 3.9, it only takes 6 iterations in both cases to obtain the converged results in spite of the increased resolution of the finite element mesh used.

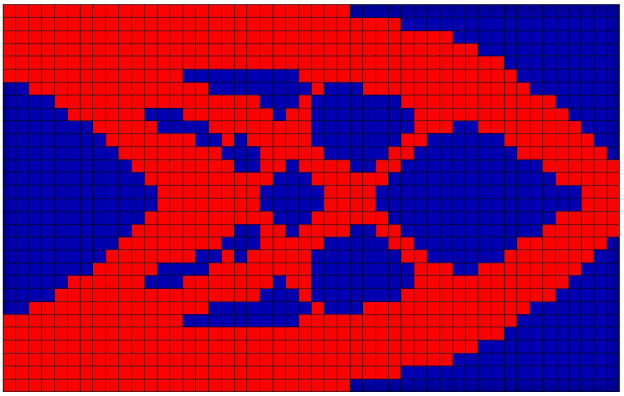

Figure 3.15. Evolved cantilever beam for static displacement objective with high resolution

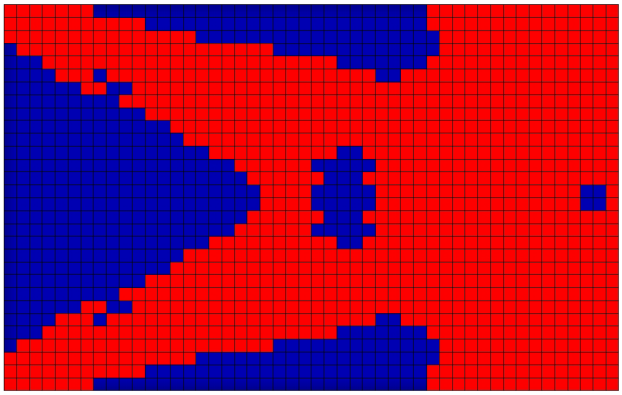

Figure 3.16. Evolved cantilever beam for modal dynamic objective with high resolution

Table 3.9. Number of iterations and volume reduction for the high resolution cantilever beam evolution

Objective	*Number of iterations*	*Volume reduction percentage*
Static: $\frac{u'}{u} = 0.5$	6	39.9%
Modal dynamic : $\frac{\omega^{2'}}{\omega^2} = 1.44$	6	33.7%

3.5. Topology Evolution with Performance Constraints Varied

Most of the topology optimization methods in the literature impose a volume constraint [3,7,15,16] while achieving maximum stiffness (i.e., compliance minimization). The ESO/LEAP algorithm developed in this work has no volume constraint since there is no limit or stopping criterion for volume reduction.

In this section, the topology evolution results using the ESO/LEAP methodology with applying different values of structural performance constraints are presented. The results show that the volume resulting in the final structure can be adjusted by applying different performance constraint values.

3.5.1. Static Displacement Constraints

The cantilever beam with a concentrated force applied at the free-end lower corner is tested for the static displacement problem. The dimension of the cantilever beam is the same as in Section 3.1, only the position of the applied force differs. Initial Young's modulus is $E_0 = 2.07 \times 10^5 MPa$, Poisson's ratio $\nu = 0.3$, and mass density $\rho = 7.833 \times 10^{-9} Ns^2 / mm^4$. A 300N force is applied downward at the corner of the free-end. A finite element mesh of 32×20 is used.

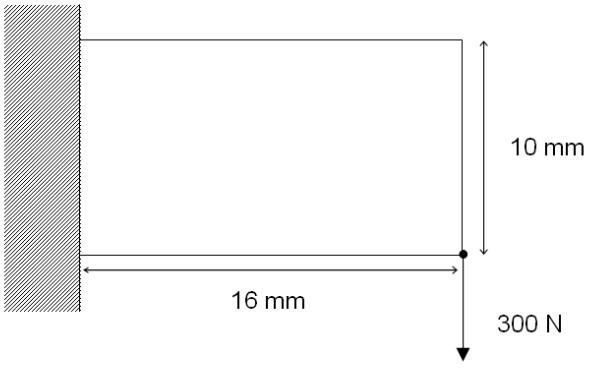

Figure 3.17. Cantilever beam with one point load at the lower corner of the free-end

The static displacement objective is to change the displacement at the loading point by a factor of 0.5, 0.65 and 0.8. The results are shown in Figure 3.18, Figure 3.19, and Figure 3.20, respectively.

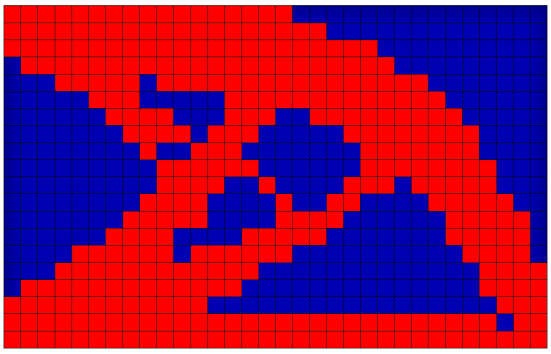

Figure 3.18. Evolved cantilever beam with lower corner force for static displacement objective $u'/u = 0.5$

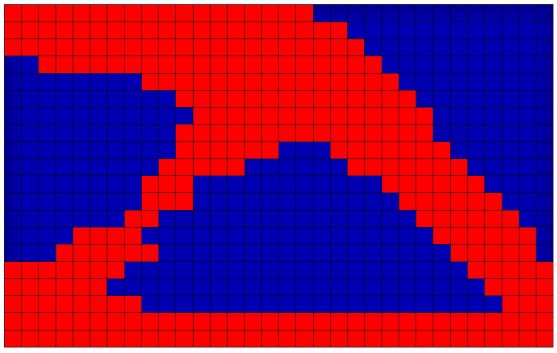

Figure 3.19. Evolved cantilever beam with lower corner force for static displacement objective $u'/u = 0.65$

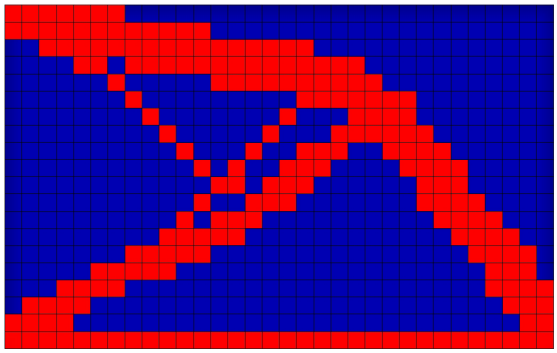

Figure 3.20. Evolved cantilever beam with lower corner force for static displacement objective $u'/u = 0.8$

Table 3.10. Number of iterations and volume reduction for static displacement objective of cantilever beam evolution with lower corner force

Objective	*Number of iterations*	*Volume reduction percentage*
Static: $\frac{u'}{u} = 0.5$	4	44.8%
Static: $\frac{u'}{u} = 0.65$	4	51.9%
Static: $\frac{u'}{u} = 0.8$	5	68.0%

We can make the following observations:

(a) By increasing the ratio of static deflection, the volume reduction rate of the objective structure increases. As expected, less material is required to design a more flexible structure.
(b) The topological branches evolve to a simple and thinner form when the static displacement constraint is more flexible.
(c) Obviously, the volume result can be adjusted by changing the value of the static displacement constraint.

3.5.2. Modal Dynamic Constraints

For the modal dynamic objective problem, same cantilever beam example is used. The objective is to increase the first eigenvalue (in-plane bending mode) by a factor of 1.44, 1.6 and 1.8. The converged results are shown in Figure 3.21, Figure 3.22 and Figure 3.23, respectively.

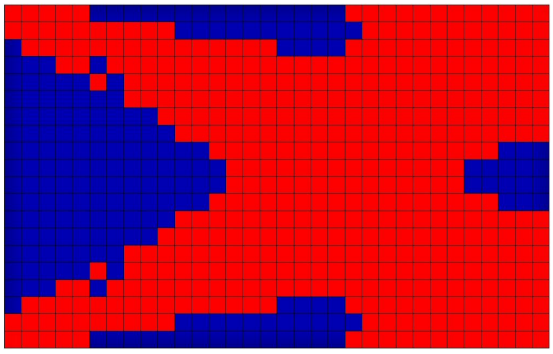

Figure 3.21. Evolved cantilever beam for modal dynamic objective $\omega^{2\prime} / \omega^2 = 1.44$

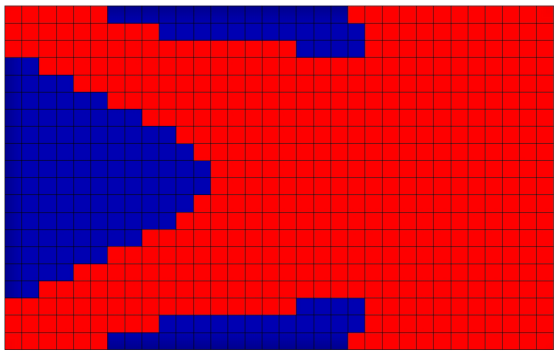

Figure 3.22. Evolved cantilever beam for modal dynamic objective $\omega^{2\prime} / \omega^2 = 1.6$

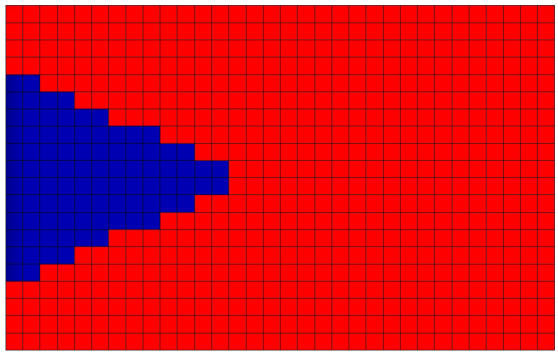

Figure 3.23. Evolved cantilever beam for modal dynamic objective $\omega^{2\prime} / \omega^2 = 1.8$

Table 3.11. Number of iterations and volume reduction for modal dynamic objective of cantilever beam evolution

Objective	*Number of iterations*	*Volume reduction percentage*
Modal dynamic : $\frac{\omega^{2'}}{\omega^2} = 1.44$	5	31.3%
Modal dynamic : $\frac{\omega^{2'}}{\omega^2} = 1.6$	3	25.9%
Modal dynamic : $\frac{\omega^{2'}}{\omega^2} = 1.8$	2	14.0%

As shown in Table 3.11, more mass remains with increasing factor of modal dynamic constraints. Intuitively, the mass should be reduced more to increase the in-plane bending mode since the eigenvalue is proportional to square root of stiffness over mass. However, the results indicate that the stiffness of the structure increases faster then the mass in the optimization process, less material is needed with increased value of the modal dynamic constraint.

CHAPTER IV

TOPOLOGY EVOLUTION PATTERNS

In this Chapter, topology evolution patterns for the examples are presented in Chapter III. Results clearly show that topological patterns develop at each iteration until convergence, while element energy is concentrated to remaining elements.

4.1. Static Displacement Topology Evolution Patterns

The static displacement topology evolution patterns are shown in this section. The objective is to decrease the displacement at the loading point by a factor of 2. It is tested using two values for E_s, 3.0 and 3.5.

4.1.1. Cantilever Beam

For the cantilever beam, the results of topology evolution are shown in Figure 4.1 and Figure 4.2 using target Young's modulus 3.0 and 3.5, respectively. Based on these results, we can make the following observations:

(a) First, the edges including the corners at which the fixed boundary condition is applied, reach the target Young's modulus (i.e., therefore freeze first). Then, element freezing propagates into the middle of the structure as the structure develops.
(b) The Gothic arch-like form appears first and then detailed shapes such as holes and branches are developed.
(c) The number of holes increases as the structure evolves toward the optimal topology.

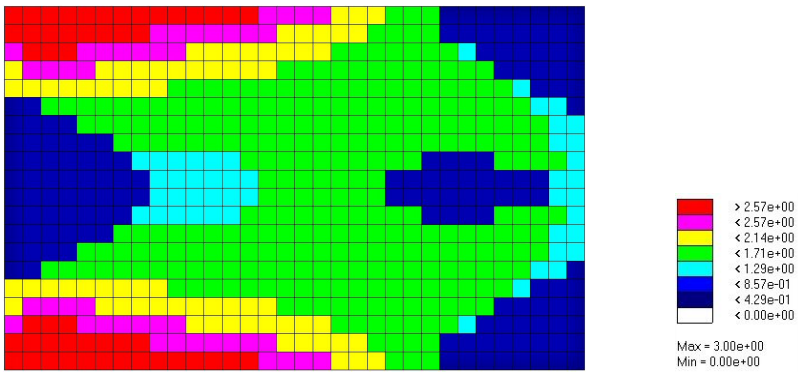

(a) Iteration 1

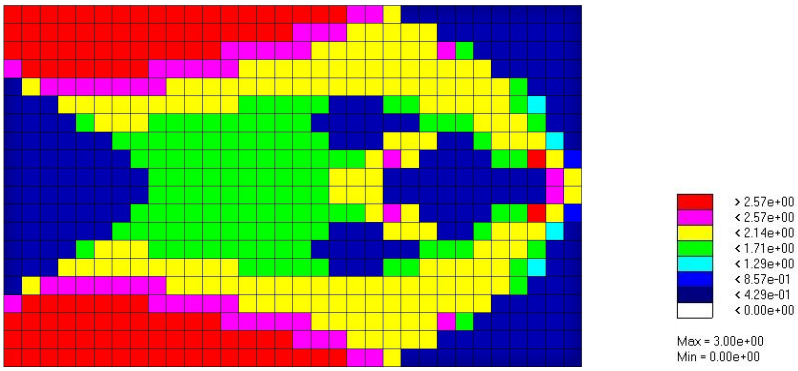

(b) Iteration 2

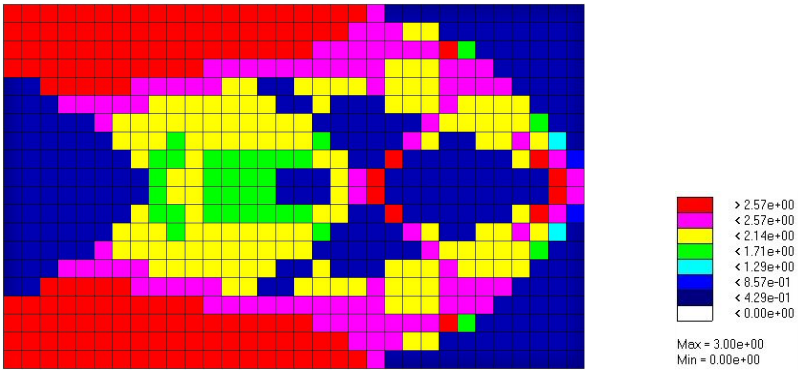

(c) Iteration 3

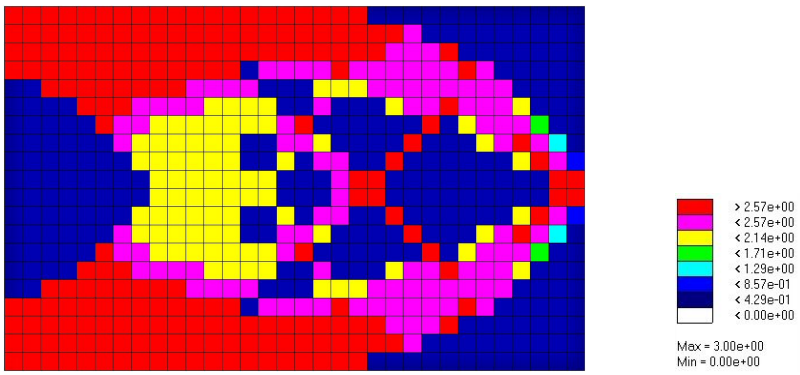

(d) Iteration 4

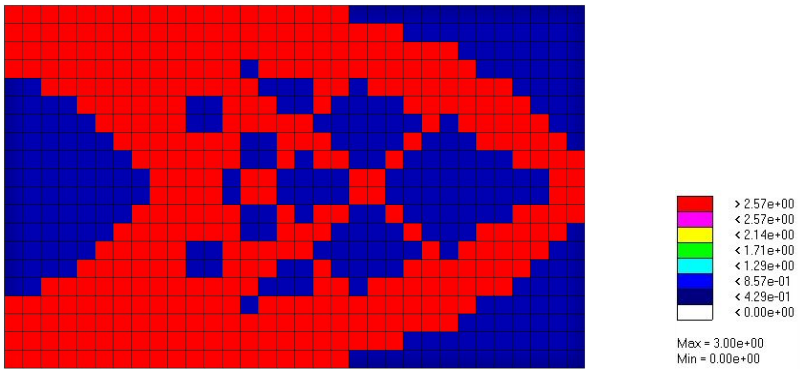

(e) Iteration 5

Figure 4.1. Topology evolution pattern for cantilever beam - static displacement objective and E_s =3.0

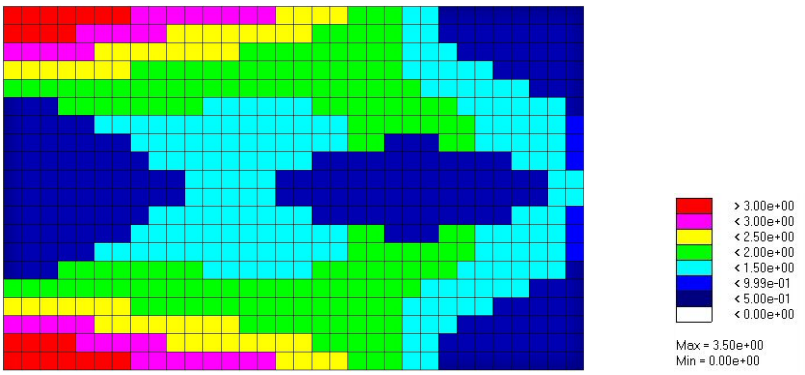

(a) Iteration 1

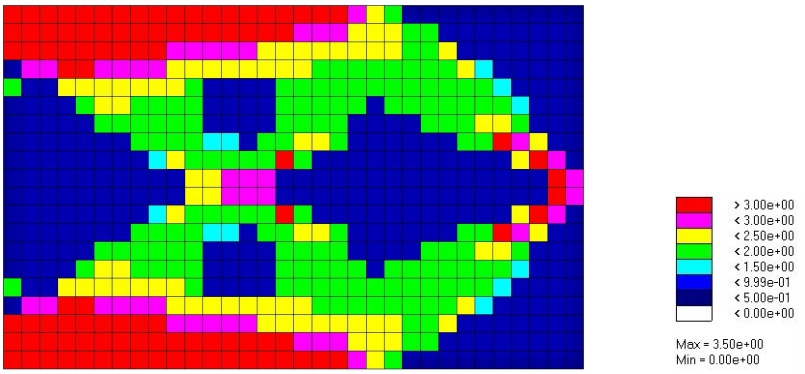

(b) Iteration 2

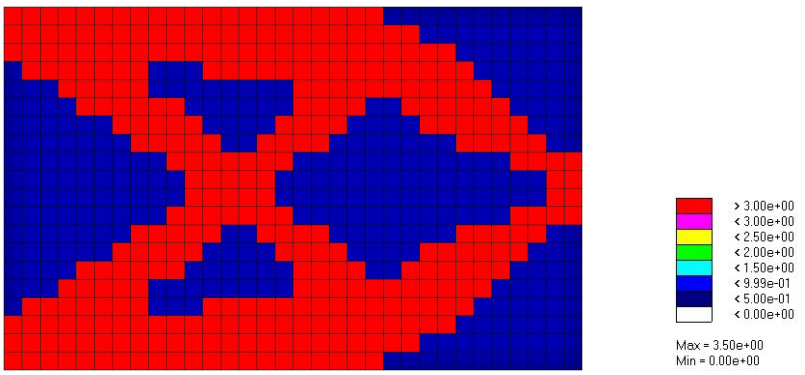

(c) Iteration 3

Figure 4.2. Topology evolution pattern for cantilever beam - static displacement objective and E_s =3.5

4.1.2. Bridge

The objective of the bridge example is to reduce the static displacement by half at mid-span of the bridge bottom, where the largest force is applied and the largest displacement occurs. The results of the topology evolution are shown in Figure 4.3 and Figure 4.4 using E_s values of 3.0 and 3.5, respectively.

(a) The simply supported ends and the top part of the bridge reach the target Young's modulus first.
(b) Three vertical structural members appear clearly as the topology evolution proceeds in both cases. These two cases show development of similar topological features, but in the stiffer material case, less material is required to support the given loads thus making the size of the voids and holes larger.
(c) The hole in the middle of the bridge emerges in the later stage of the evolving process.

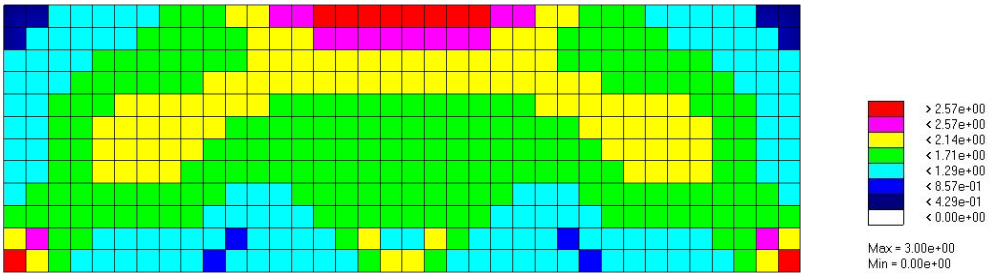

(a) Iteration 1

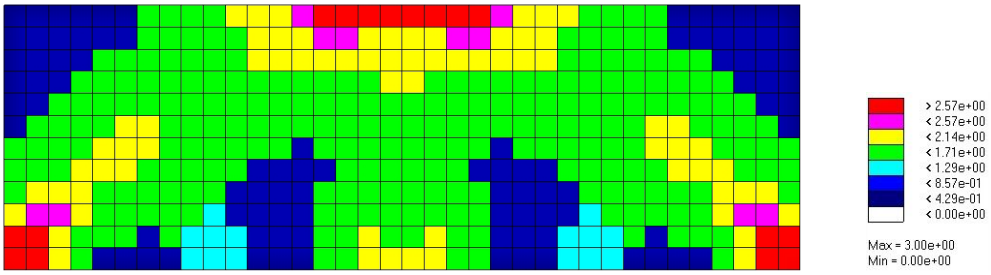

(b) Iteration 2

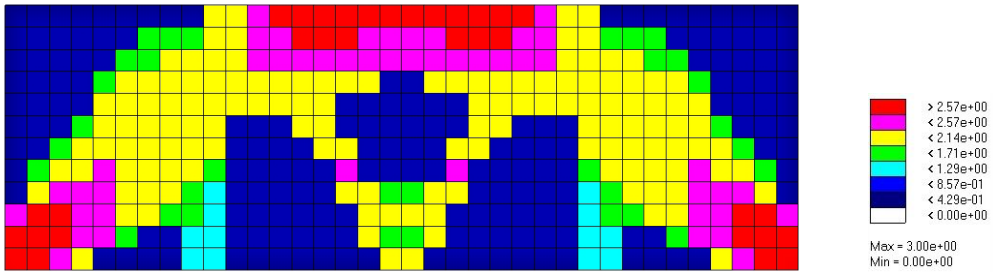

(c) Iteration 3

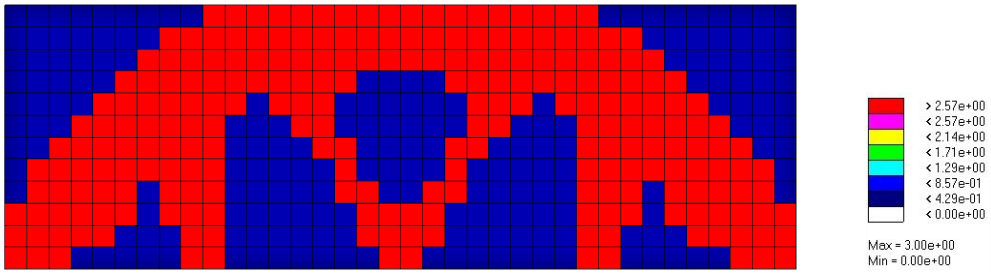

(d) Iteration 4

Figure 4.3. Topology evolution pattern for bridge - static displacement objective and E_s =3.0

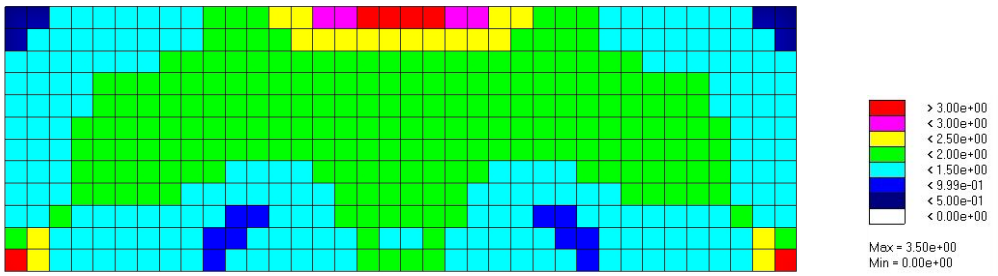

(a) Iteration 1

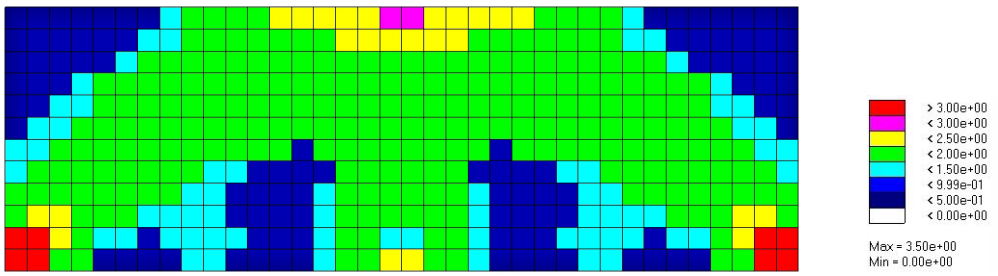

(b) Iteration 2

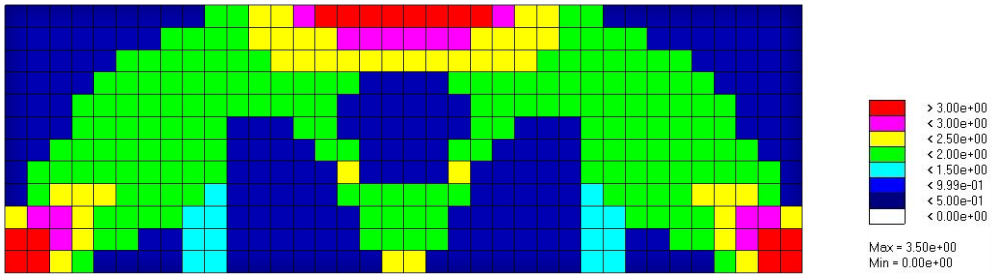

(c) Iteration 3

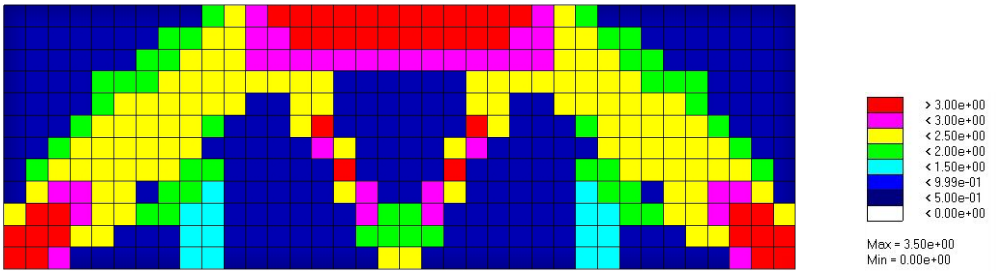

(d) Iteration 4

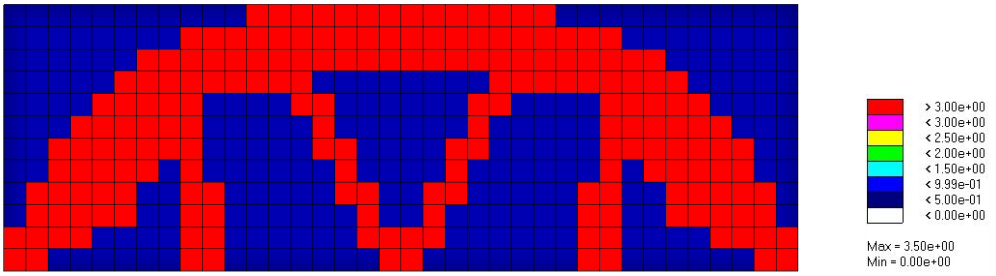

(e) Iteration 5

Figure 4.4. Topology evolution pattern for bridge - static displacement objective and E_s =3.5

4.2. Modal Dynamic Topology Evolution Patterns

The objective of modal dynamic example is to increase the first eigenvalue which corresponds to the in-plane bending. For the cantilever beam, the objective is to increase by the factor of 1.44 and for the bridge the objective is to increase by a factor of 2.0.

4.2.1. Cantilever Beam

Figure 4.5 and Figure 4.6 show the topology evolution for the modal dynamic constraints using different target Young's modulus E_s of 3.0 and 3.5, respectively. The resulting topology exhibits the following features:

(a) At first, the clamped corners of the left side of the structure reach the target Young's modulus. Then, the remaining elements are frozen in the middle of the structure as the structure evolves to the objective design.
(b) The material near the free-end almost remains intact during the evolution process. This provides the mass needed to achieve modal dynamic goals while voids appear close to the clamped end.
(c) Both cases E_s of 3.0 and 3.5 exhibits very similar topological development process, while using higher E_s value results in two small holes in the center of the structure in the later stage of the evolution.

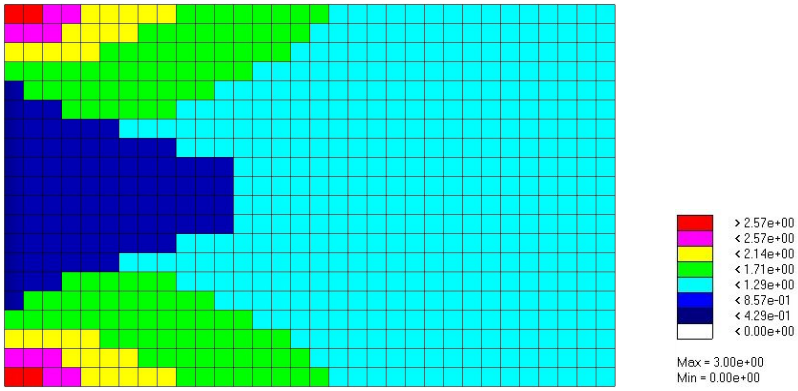

(a) Iteration 1

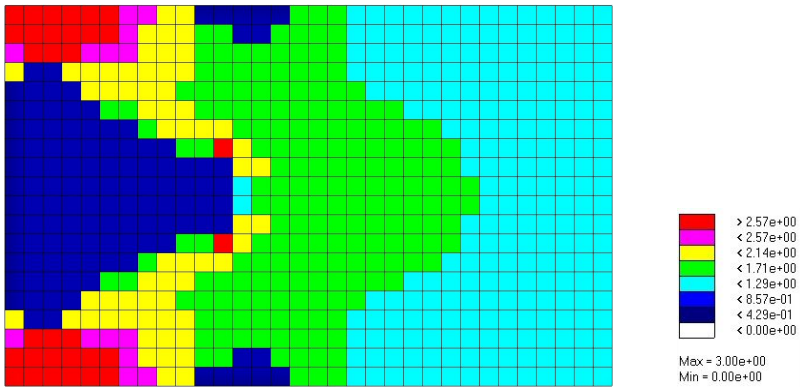

(b) Iteration 2

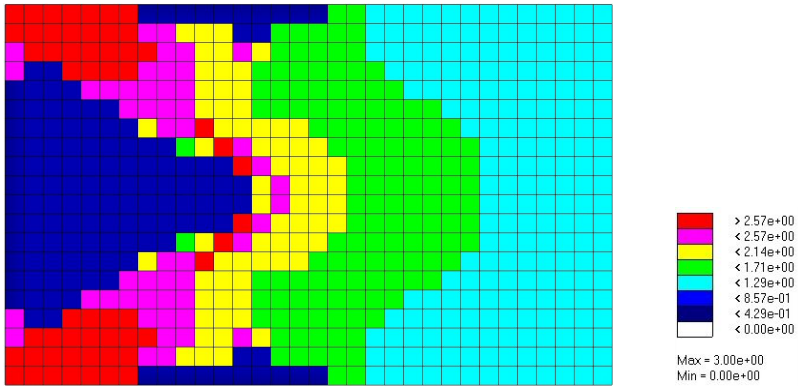

(c) Iteration 3

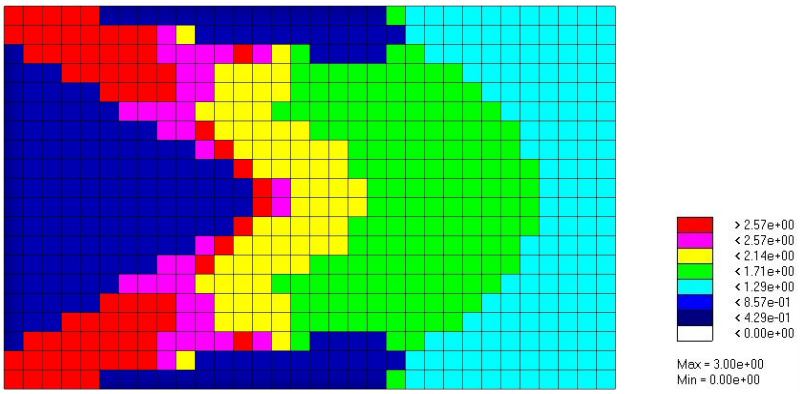

(d) Iteration 4

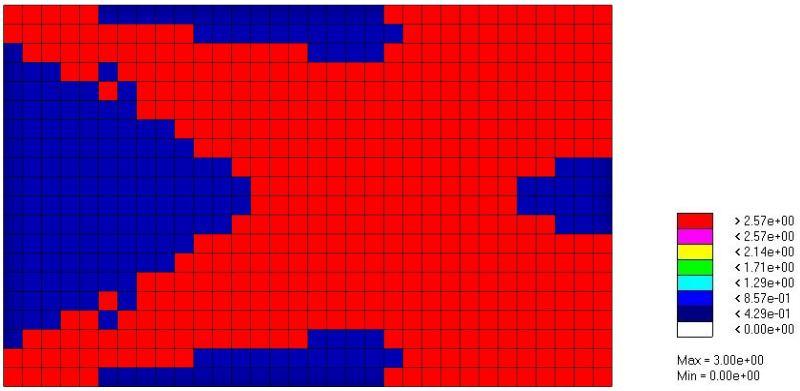

(e) Iteration 5

Figure 4.5. Topology evolution pattern for cantilever beam – modal dynamic objective and E_s =3.0

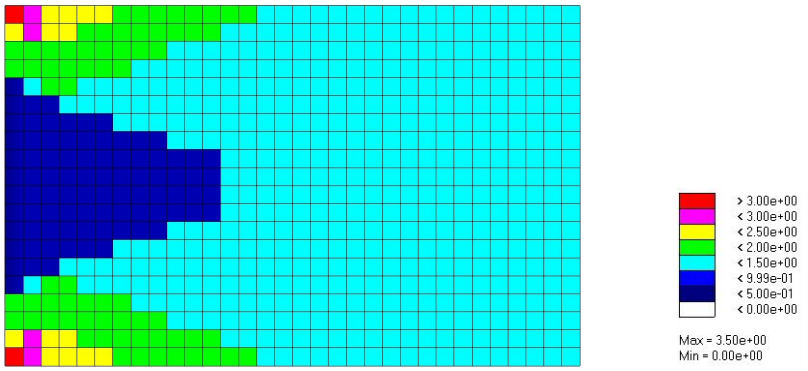

(a) Iteration 1

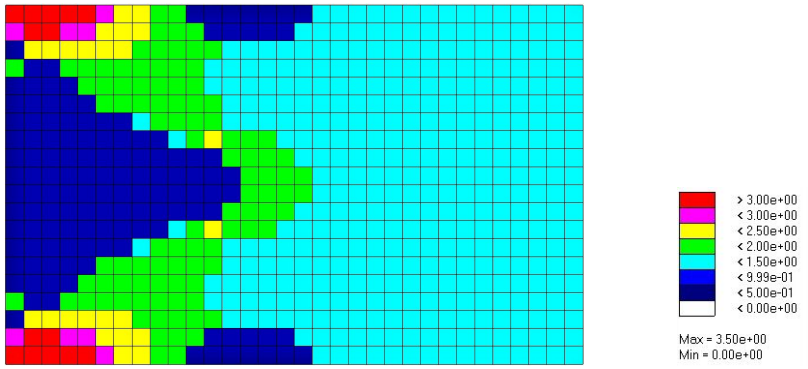

(b) Iteration 2

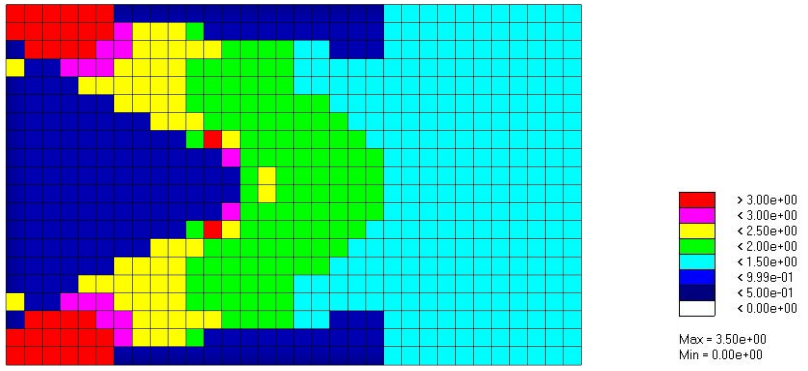

(c) Iteration 3

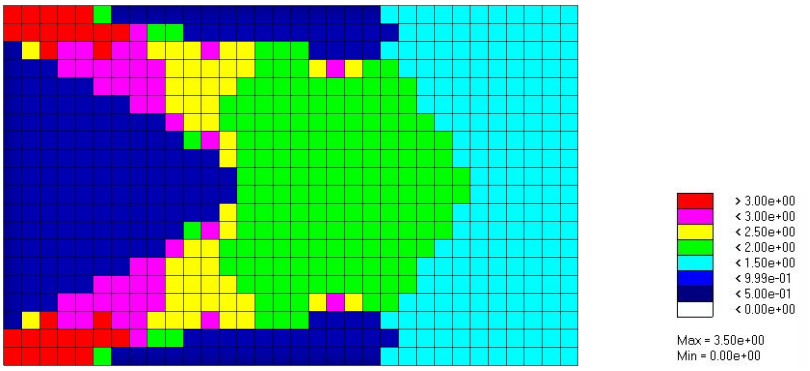

(d) Iteration 4

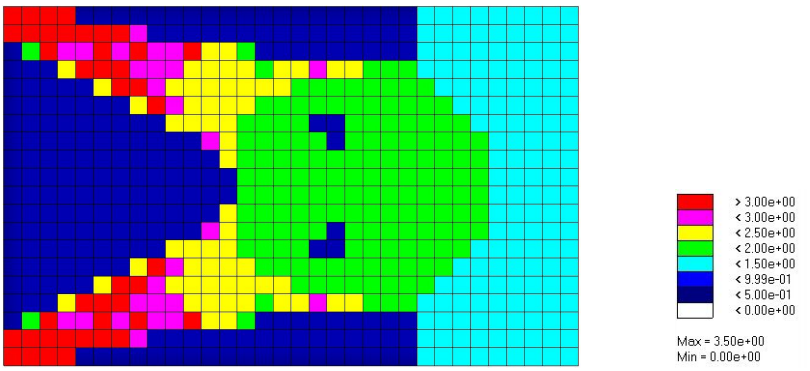

(e) Iteration 5

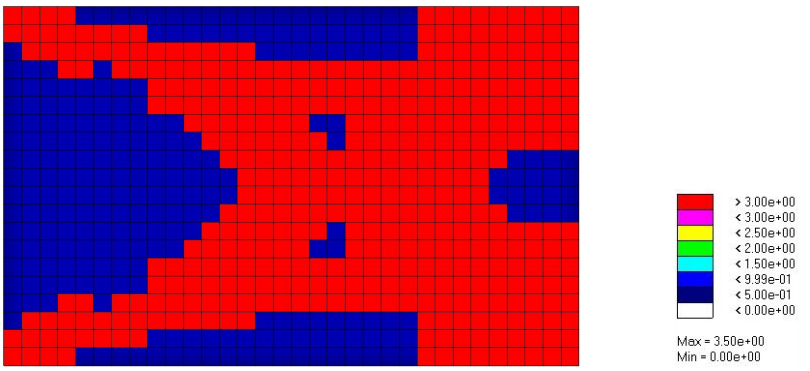

(f) Iteration 6

Figure 4.6. Topology evolution pattern for cantilever beam – modal dynamic objective and E_s =3.5

4.2.2. Bridge

For the bridge example, the modal dynamic objective is to increase the first eigenvalue by a factor of 2.0. The results of topology evolution are depicted in Figure 4.7 and Figure 4.8. The resulting topology exhibits the following features.

(a) For both cases, the mass is preserved in the middle of the structure throughout the evolution process.
(b) The topological evolution is similar for both cases. However, the holes near the end supports appear in the last iteration for the higher target Young's modulus E_s case.

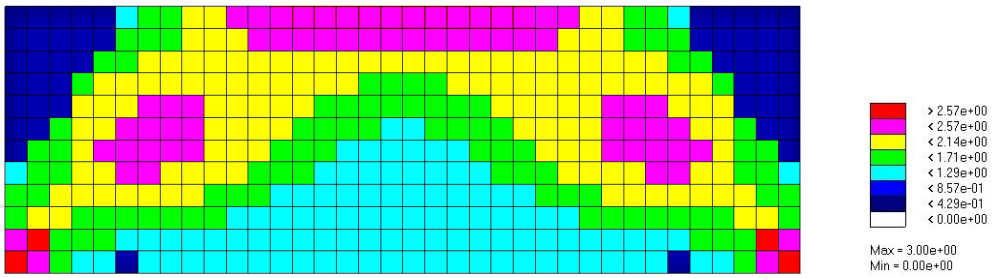

(a) Iteration 1

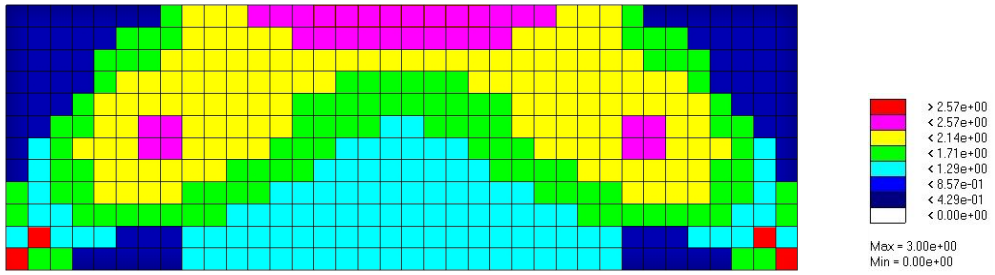

(b) Iteration 2

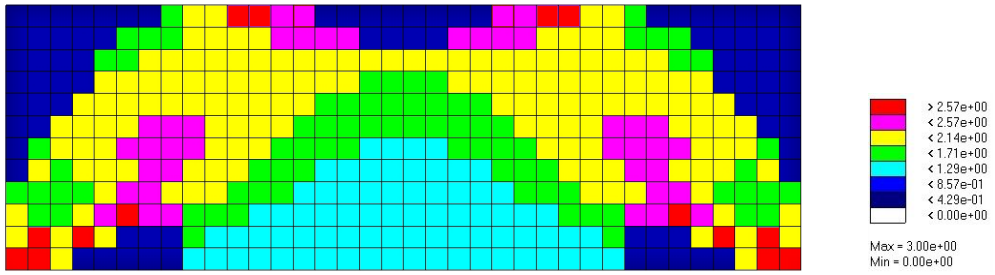

(c) Iteration 3

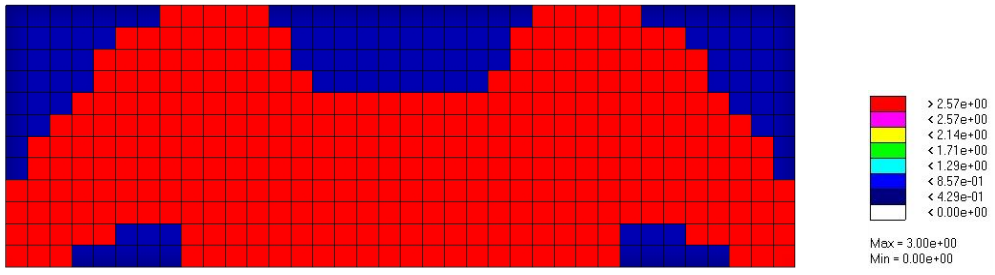

(d) Iteration 4

Figure 4.7. Topology evolution pattern for bridge – modal dynamic objective and E_s =3.0

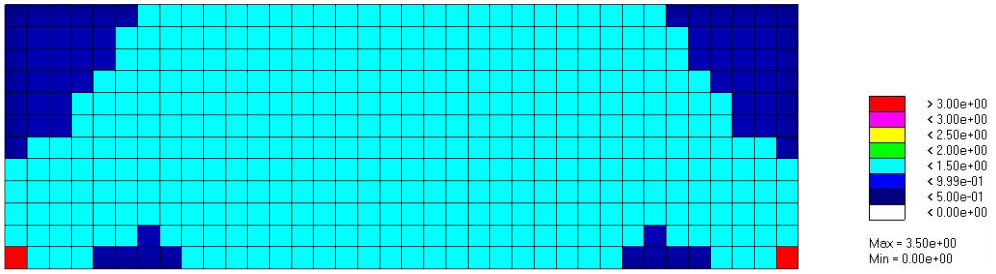

(a) Iteration 1

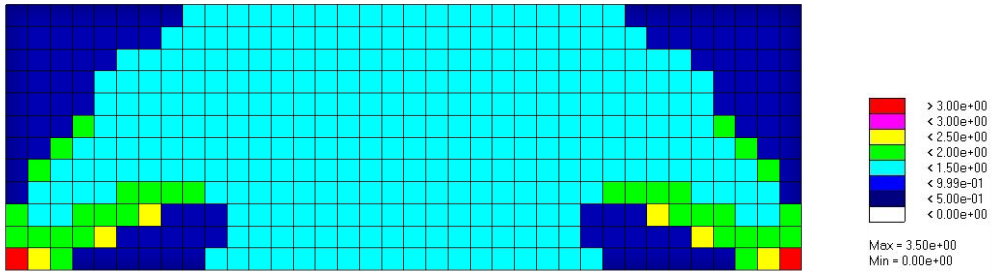

(b) Iteration 2

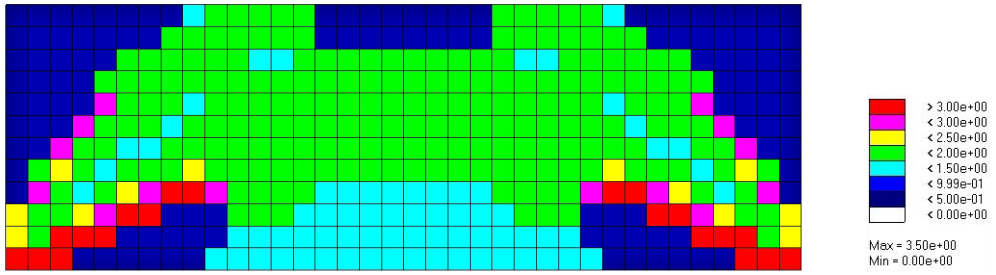

(c) Iteration 3

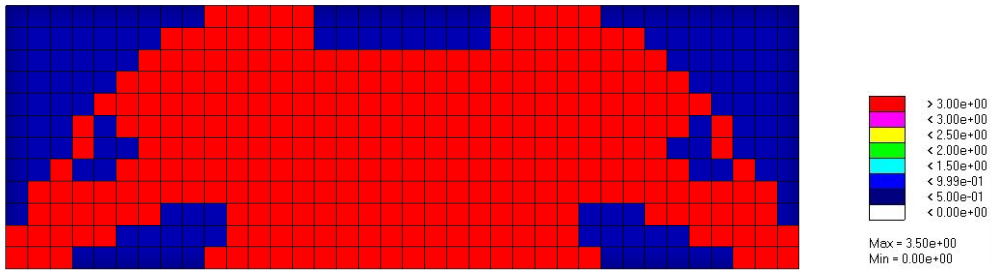

(d) Iteration 4

Figure 4.8. Topology evolution pattern for bridge – modal dynamic objective and E_s =3.5

4.3. Static and Modal Dynamic Topology Evolution Patterns

In this section, static displacement and modal dynamic objectives are achieved at the same time. As in Table 3.1, the objectives for the cantilever beam are to reduce the displacement of a loading point at the center of the free-end by a factor of 0.65 and to increase the in-plane bending mode by a factor of 1.44 simultaneously. For the bridge example, the objective is to decrease the mid-span of the bridge bottom by a factor of 0.6 and to increase the first eigenvalue by a factor 1.8.

4.3.1. Cantilever Beam

Figure 4.9 and Figure 4.10 show the results of cantilever beam example with static displacement and modal dynamic constraints using E_s as 3.0 and 3.5, respectively. Based on these results, we can make the following observations:

(a) For both cases, the structural topology develops from the edge of the fixed boundary and propagates to the free-end similar to the static displacement topology evolution patterns.
(b) The mass near the free-end mostly remains throughout the evolving process.
(c) Gothic-arch form develops gradually while the mass shifts to the free-end to maintain the modal dynamic characteristics.
(d) For E_s =3.5 case, a large void appears half-way through evolution process which makes the objective structure look like combined topology of the static and the modal dynamic examples.

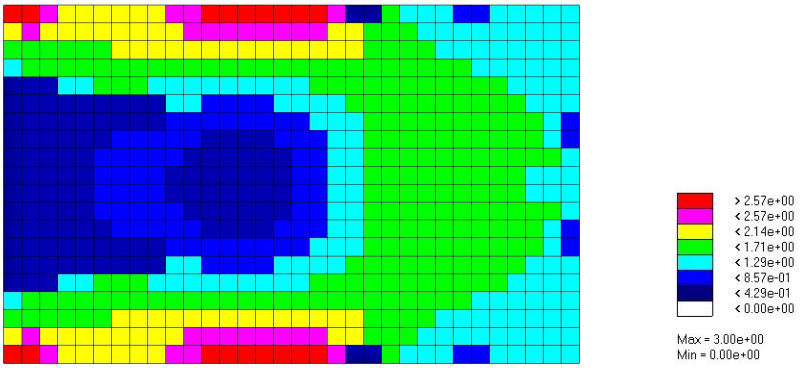

(a) Iteration 1

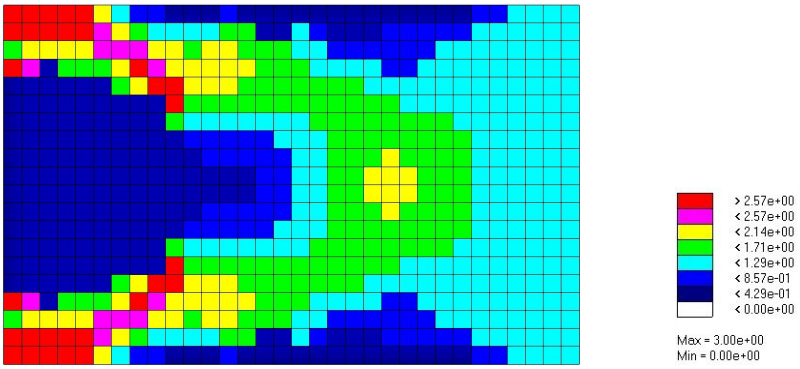

(b) Iteration 2

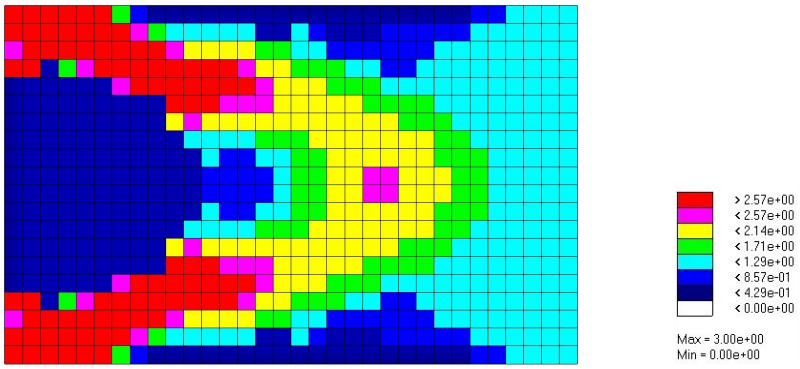

(c) Iteration 3

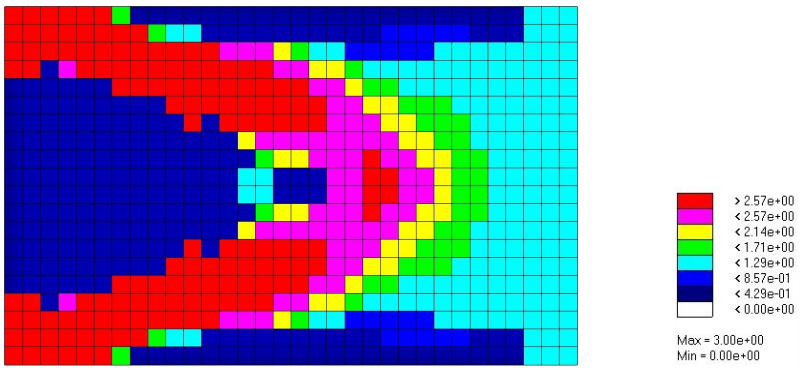

(d) Iteration 4

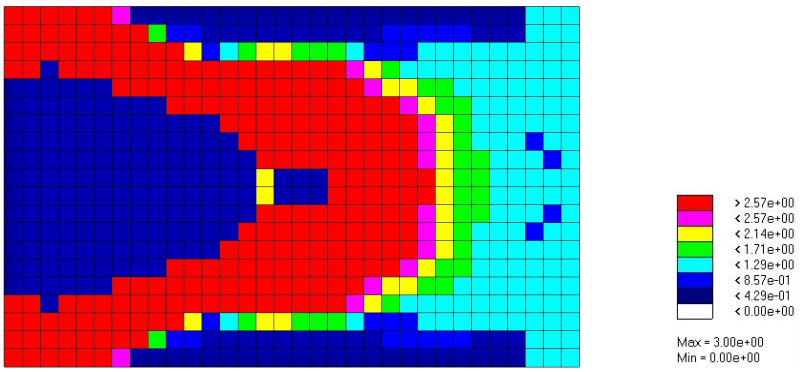

(e) Iteration 5

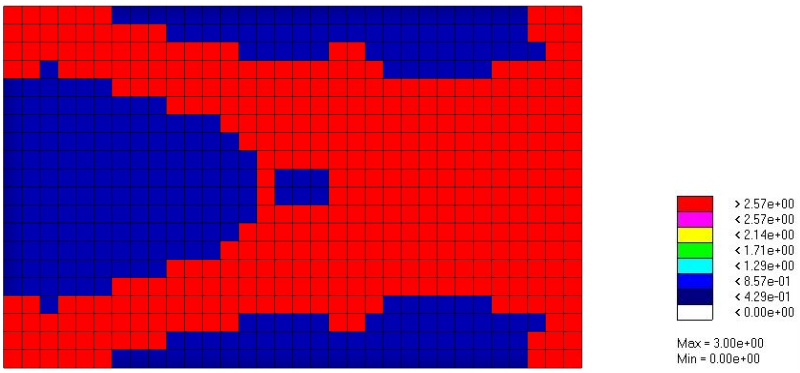

(f) Iteration 6

Figure 4.9. Topology evolution pattern for cantilever beam – static displacement/modal dynamic objectives and E_s =3.0

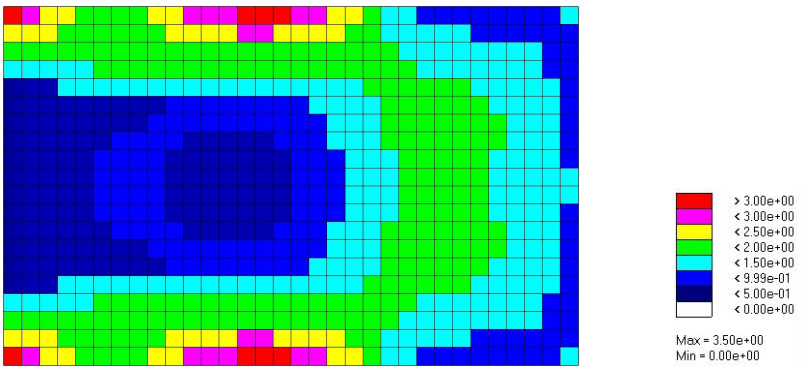

(a) Iteration 1

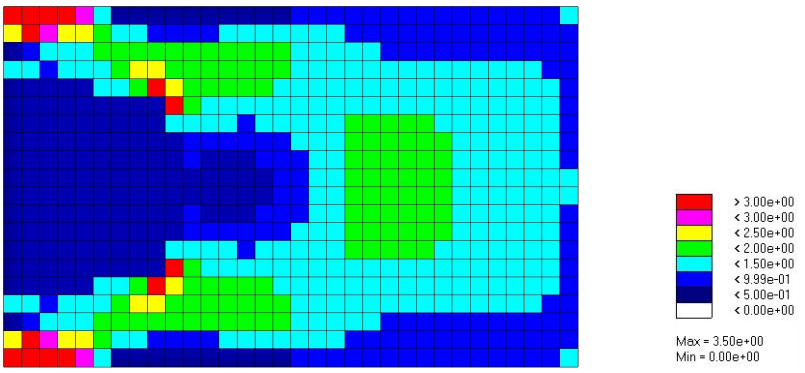

(b) Iteration 2

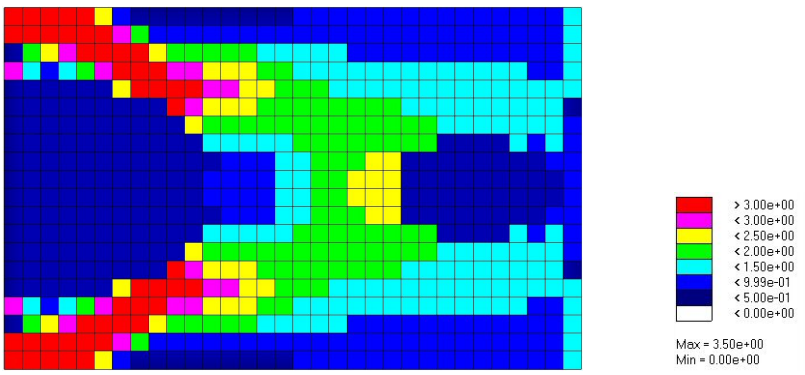

(c) Iteration 3

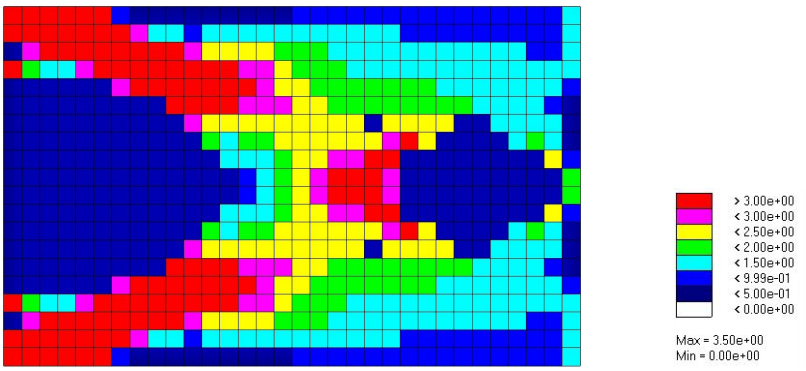

(d) Iteration 4

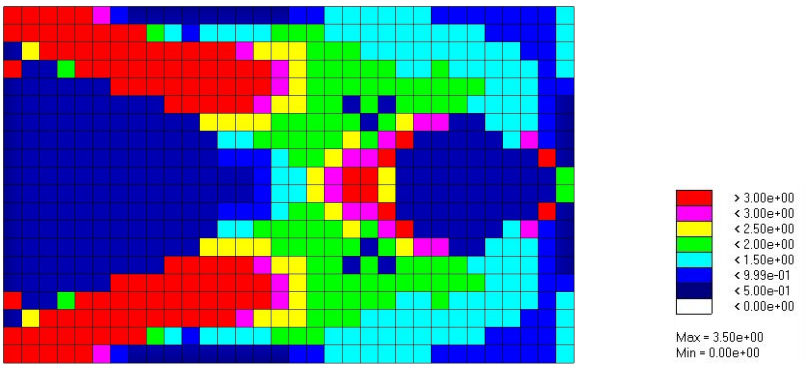

(e) Iteration 5

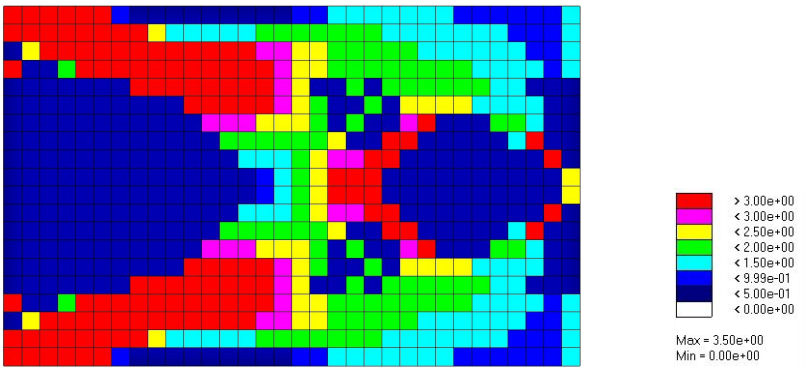

(f) Iteration 6

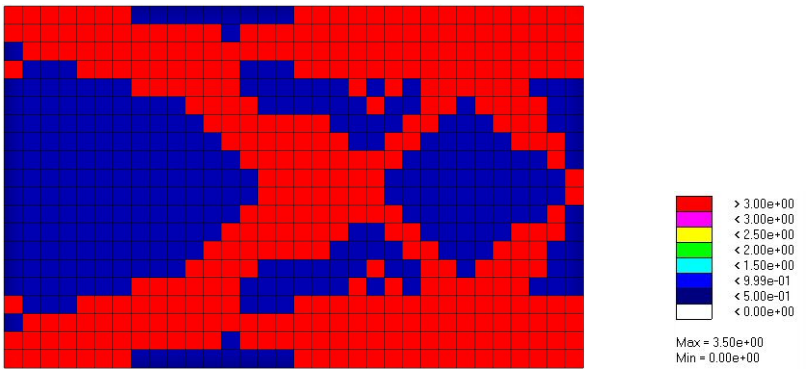

(g) Iteration 7

Figure 4.10. Topology evolution pattern for cantilever beam – static displacement/modal dynamic objectives and E_s =3.5

4.3.2. Bridge

For the bridge example, the evolved topology using target Young's modulus 2.0 and 2.5 is shown in Figure 4.11 and Figure 4.12. For both cases, the results show similar topology evolution patterns.

(a) The top part of the bridge and the end supports develop first, and then to the center of the bridge. This occurs also in the static displacement example.
(b) The arch shape appears clearly from the early stage of evolutionary process and remains to the end while detailed holes emerge in the later stage of the evolution process.
(c) For the stiffer material case, the holes become larger and larger as the iteration step proceeds.

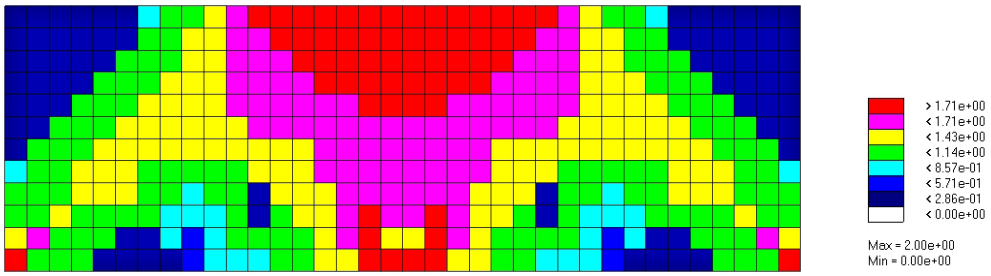

(a) Iteration 1

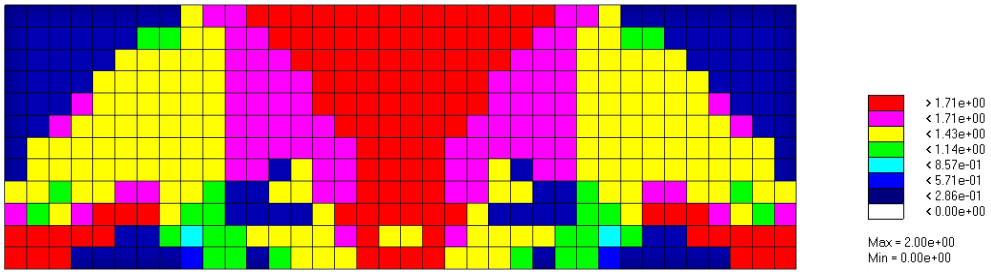

(b) Iteration 2

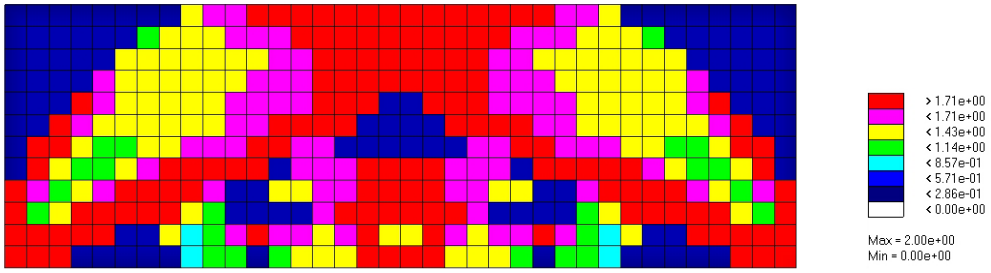

(c) Iteration 3

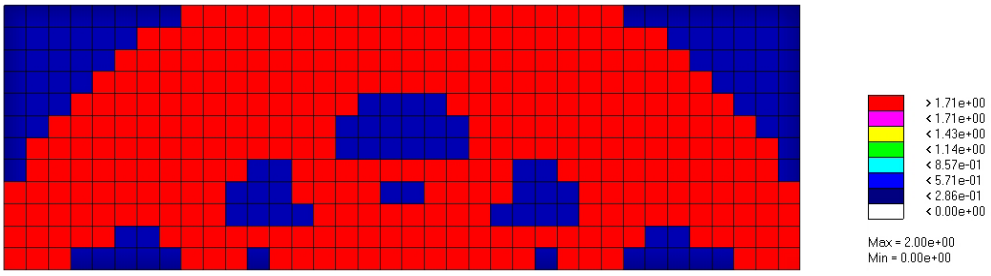

(d) Iteration 4

Figure 4.11. Topology evolution pattern for bridge – static displacement/modal dynamic objectives and E_s =2.0

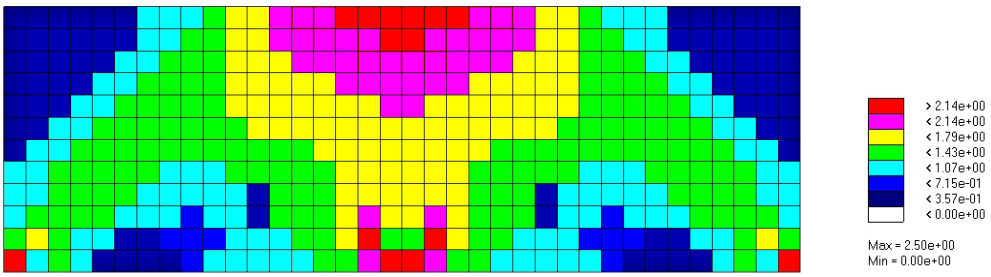

(a) Iteration 1

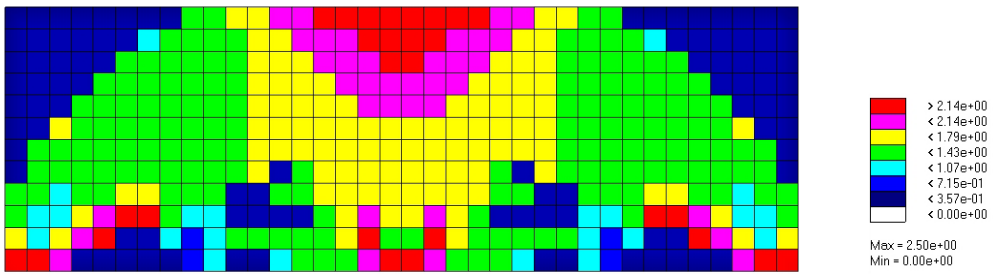

(b) Iteration 2

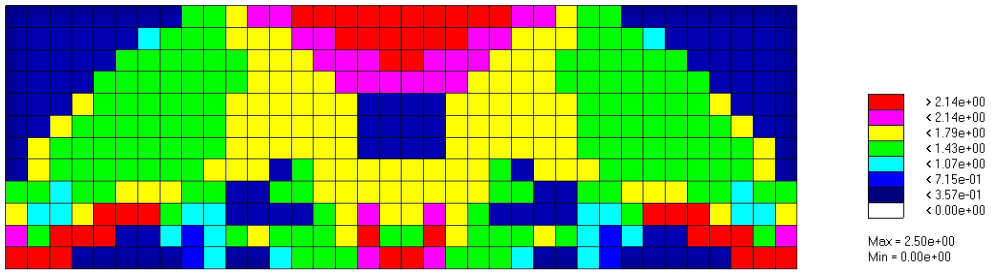

(c) Iteration 3

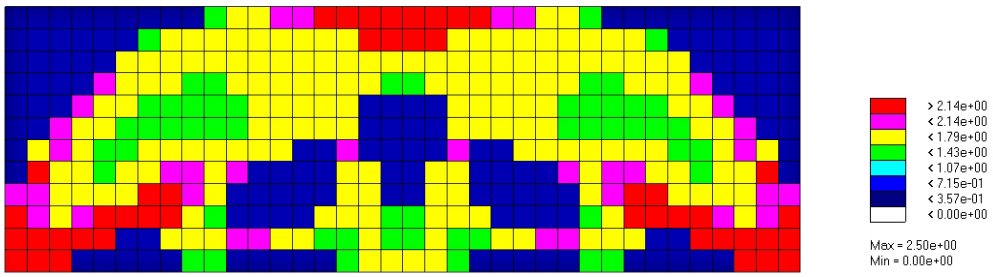

(d) Iteration 4

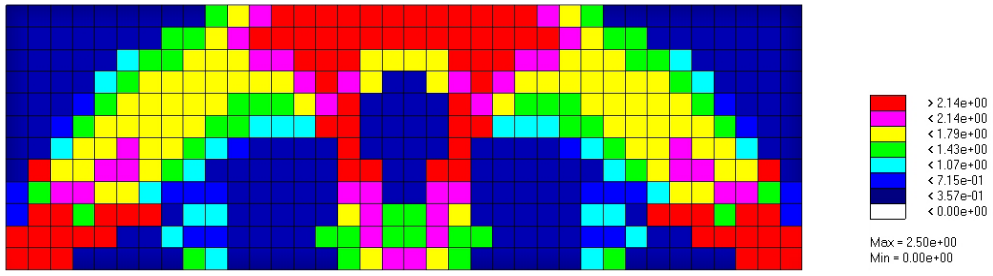

(e) Iteration 5

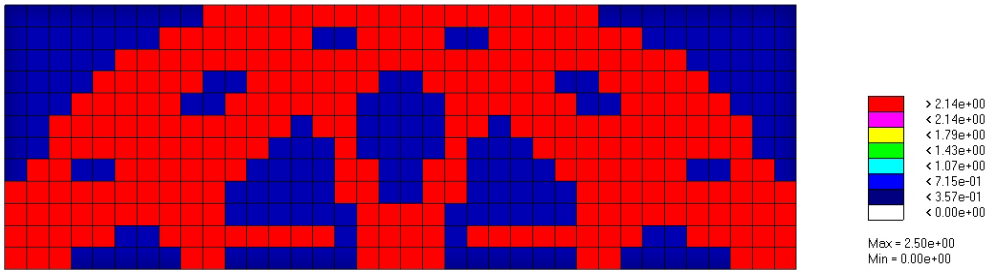

(f) Iteration 6

Figure 4.12. Topology evolution pattern for bridge – static displacement/modal dynamic objectives and E_s =2.5

CHAPTER V

CONCLUSIONS

In this dissertation, a topology evolution algorithm for Evolutionary Structural Optimization (ESO) using LargE Admissible Perturbations (LEAP) was developed, implemented and tested. In Section 5.1, the dissertation contributions are summarized. A series of concluding remarks is given in Section 5.2. Finally, in Section 5.3, suggested future research is recommended.

5.1. Dissertation Contributions

The main contributions of the present work can be summarized as follows:

(1) The ESO methodology as described in the literature cannot handle multicriterion constraints efficiently. There was only a single attempt to solve minimization of mean compliance (maximization of stiffness) and maximizing first natural frequency simultaneously using Evolutionary Structural Optimization (ESO) with the weighting method [14]. However, the results are limited to presenting different topological structures by varying weighting criteria, not achieving a specific value of performance constraints. The LargE Admissible Perturbation (LEAP) methodology handles multiple performance constraints and therefore the ESO developed in this thesis is not subject to the above limitation.

(2) Previous ESO methods use material density ρ set equal to 0 or 1 as design variable. They cannot vary Young's modulus and can only use initial Young's modulus of a fixed value. But ESO using LEAP methodology allows to change Young's modulus

to achieve better structural performance with various Young's modulus values while at the same time eliminating mass as needed.

(3) Most methodologies for topology optimization in the literature require 40 to 100 numerical iterations. Current topology optimization methods using ESO still require at least 60~70 iterations to converge [15], while ESO using the LEAP methodology only takes 3 to 7 iterations to obtain converged results, thus, showing advanced computational efficiency.

(4) Stabilized the optimization algorithm and improved computational efficiency by developing the Cumulative Energy Elimination Rate (*CEER*) scheme. Compared to the results of using fixed rate elimination method, less number of iterations is achieved by developing the *CEER* scheme. If the fixed rate elimination scheme is applied, convergence is not always guaranteed because there is a possibility that it might remove some useful elements causing the structure to disappear in the later stage of the evolution process.

(5) Most of the topology optimization methods in the literature impose volume constraints while setting minimizing compliance as objective function. Since the ESO/LEAP methodology does not have volume constraints, it was difficult to compare the results of the current methodology to other topology optimization results. In this work, numerical examples are used to show that the volume can be adjusted by controlling performance constraint values. The results of ESO/LEAP methodology can be related to results of other methods by changing the values of performance constraints.

(6) Similar topological results can be obtained with increased number of elements in finite element analysis still achieving advanced computational efficiency. Benchmark examples were tested to show that the result using higher resolution finite element mesh exhibit very similar characteristics compared to coarse mesh examples still with few iterations of finite element analysis required for convergence.

5.2. Concluding Remarks

An Evolutionary Structural Optimization algorithm using the Large Admissible Perturbation method was developed. The cumulative energy elimination scheme was proposed to remove the ineffective finite elements at each iteration. The advantages of the current method can be summarized as: (1) ESO using the LEAP methodology presented in this work can achieve an optimal topology that satisfies single/multiple objectives with very few iterations and only two finite element analyses per iteration. It only takes as few as 3 to 7 iterations to obtain converged results showing advanced computational efficiency. (2) The ESO/LEAP methodology can handle multiple performance design objectives such as static displacement and modal dynamic. Unlike the other ESO/BESO methods reported in the literature, the current method can deal with multiple objectives effectively since the LEAP methodology handles multiple performance constraints. (3) ESO/LEAP can vary the target material stiffness, which allows a designer to obtain various evolved structures satisfying multiple design constraints. (4) Implementing the Cumulative Energy Elimination Rate (*CEER*) scheme stabilized the optimization algorithm and improved computational efficiency. Compared to the results of using fixed rate elimination method, smaller number of iterations is achieved by developing the *CEER* scheme. (5) Showed that volume can be adjusted by controlling performance constraints values in ESO/LEAP methodology. The results of the current methodology can be related to other topology optimization results in the literature which usually impose volume constraints. (6) Similar results are obtained with increased number of mesh in finite element analysis still achieving advanced computational efficiency.

Two benchmark applications, cantilever beam and bridge, are presented with multiple numerical applications to show the effectiveness of the developed methodology. The topological features of the results can be justified intuitively depending on the performance objectives.

The ESO methodology as described in the literature cannot handle multicriterion constraints efficiently. There has been only a single attempt to solve minimization of

mean compliance (maximization of stiffness) and maximizing first natural frequency simultaneously using Evolutionary Structural Optimization (ESO) with the weighting and global criterion method (Proos K.A., et al.[14]). However, the results are limited to presenting different topological structures by varying weighting criteria, not achieving specific values of performance constraints. The LargE Admissible Perturbation (LEAP) methodology handles multiple performance constraints and therefore the ESO developed in this work is not subject to the above limitation.

5.3. Suggested Future Work

The following future research is recommended:

(1) Improve ESO/LEAP methodology with Bi-directional Evolutionary Structural Optimization. The present algorithm developed is based on only elimination of low energy elements starting from a solid block structure. It cannot impose volume constraints as target objectives like other ESO algorithms. By applying Bi-directional Evolutionary Structural Optimization to the ESO/LEAP method, robustness can be further enhanced.

(2) Extend the ESO/LEAP methodology with additional structural constraints. In the present cases, the performance constraints applied were static displacement and modal dynamic only. New and richer structural topologies can be created imposing other constraints such as static stress and forced response amplitudes applied independently or in combinations.

(3) Improve the nonlinear optimization process in order to deal with much larger number of variables and constraints. The current FSQP (Feasible Sequential Quadratic Programming) algorithm does not provide sufficient options to adjust the optimization process in case of failure to search for converging solutions.

APPENDIX A

General Perturbation Equation for Static Deflection with Static Mode Compensation

The following derivation is based on the work of Bernitsas and Suryatama [25].

(a) Static Mode Compensation

Assuming that $\{f'\} = \{f\}$ which implies that f does not depend on allowed geometric changes (α_e's), the static equilibrium equation of the unknown State S2 can be written as

$$[k']\{u'\} = \{f\}, \tag{A.1}$$

Define $\{Q'\}$ as transformed displacement vector, then the predicted static deflection $\{u'\}$ can be approximated by including the static deflection mode of the baseline structure $\{u\}$.

$$\{u'\} = \{u\} + [\Phi']\{Q'\}, \tag{A.2}$$

where $[\Phi']$ is the matrix of the mode shape vectors of the unknown State S2 which are $[\Phi'] = [\{\phi'\}_1, \{\phi'\}_2, \cdots, \{\phi'\}_{n_r}]$.

Substituting (A.2) into (A.1) gives

$$[k']\{u\} + [k'][\Phi'][Q'] = \{f\} \tag{A.3}$$

Premultiply (A.3) by $[\Phi']^T$ yields

$$[\Phi']^T[k']\{u\} + [\Phi']^T[k'][\Phi']\{Q'\} = [\Phi']^T\{f\} \tag{A.4}$$

Since the generalized stiffness matrix is defined as

$$[K'] = [\Phi']^T[k'][\Phi'], \tag{A.5}$$

And equation (A.4) can be written as

$$[K']\{Q'\} = [\Phi']^T\{f\} - [\Phi']^T[k']\{u\} \tag{A.6}$$

Using equation (2.19), equation (A.6) can be rewritten as

$$[K']\{Q'\} = -[\Phi']^T[\Delta k]\{u\} \tag{A.7}$$

Premultiplying each side by $[K']^{-1}$ which is equal to $[1/K']$, gives the following equation for the transformed displacement vector $\{Q'\}$,

$$\{Q'\} = -[1/K'][\Phi']^T[\Delta k]\{u\} \tag{A.8}$$

Substituting equation (A.8) into (A.2) yields the predicted static deflection in a form that includes no matrix inversion

$$\{u'\} = \{u\} - [\Phi'][1/K'][\Phi']^T[\Delta k]\{u\} \tag{A.9}$$

(b) General Perturbation Equation for Static Deflection Redesign

From equation (2.25) and (A.8), the components of the displacement vector $\{u'\}$ can be obtained as

$$u_i' = u_i - \sum_{m=1}^{n_r} \left\{ \frac{\phi_{i,m}'}{K_m'} \left(\sum_{e=1}^{p} (\{\phi'\}_m^T [k_e] \{u\} \alpha_e) \right) \right\} \tag{A.10}$$

where $\{\phi_m'\}$ and $\phi_{i,m}'$ are a dynamic mode and its component in the i th degree of freedom, n_r is the number of extracted modes, and p is the total number of redesign variables.

Using the equation (2.19), (A.5) can be rewritten as

$$[K'] = [\Phi']^T [k] [\Phi'] + [\Phi']^T [\Delta k] [\Phi'] \tag{A.11}$$

Then for each eigenvector m, equation (A.11) becomes

$$K_m' = \{\phi'\}_m^T [k] \{\phi'\}_m + \sum_{e=1}^{p} (\{\phi'\}_m^T [k_e] \{\phi'\}_m) \alpha_e \tag{A.12}$$

Substituting (A.12) into (A.10) gives

$$u_i' = u_i - \sum_{m=1}^{n_r} \phi_{i,m}' \frac{\sum_{e=1}^{p} \{\phi'\}_m^T [k_e] \{u\} \alpha_e}{\{\phi'\}_m^T [k] \{\phi'\}_m + \sum_{e=1}^{p} (\{\phi'\}_m^T [k_e] \{\phi'\}_m) \alpha_e}, \text{ for } i, j = 1, 2, ..., n \tag{A.13}$$

which is the general perturbation equation for static deflection with static mode compensation.

Let $A_{me} = \{\phi'\}_m^T [k_e]\{u\}$, $B_m = \{\phi'\}_m^T [k]\{\phi'\}_m$ and $C_{me} = \{\phi'\}_m^T [k_e]\{\phi'\}_m$,

Then equation (A.13) can be written as more compact form as

$$u_i' = u_i - \sum_{m=1}^{n_r} \phi_{i,m}' \frac{\sum_{e=1}^{p} A_{me}\alpha_e}{B_m + \sum_{e=1}^{p} C_{me}\alpha_e} \tag{A.14}$$

APPENDIX B

General Perturbation Equation for Modal Dynamics

Define generalized mass matrix of the objective structure as

$$[M'] = [\Phi']^T [m'][\Phi'] \tag{B.1}$$

where $[\Phi']$ is the matrix of the mode shape vectors of the unknown State S2.

Also define the structural perturbations for eigenvalues as

$$[\omega'^2] = [\omega^2] + [\Delta\omega^2] \tag{B.2}$$

Premultiplying $[\Phi']^T$ to equation (2.18) gives the modal equation for the unknown State S2.

$$[K'] = [M'][\omega'^2] \tag{B.3}$$

Substituting the equations (2.19)-(2.21), (B.2) and (2.25)-(2.26) which are the linear relationships of α_e between stiffness and mass matrix into (B.3), we get

$$\sum_{e=1}^{p} (\{\phi'\}_j^T [k_e] \{\phi'\}_i - \omega_i^2 \{\phi'\}_j^T [m_e] \{\phi'\}_i^T) \alpha_e = \omega_i'^2 \{\phi'\}_j^T [m] \{\phi'\}_i - \{\phi'\}_j^T [k_e] \{\phi'\}_i ,$$

$$\text{for } i, j = 1, 2, ..., n \tag{B.4}$$

which is the general perturbation equation for modal dynamics. n is the number of degrees of freedom of the finite element modal in the initial state S1.

The equation (B.4) can be separated into two groups, Diagonal, that is $i = j$ terms, which represent the Rayleigh quotient for mode i, and the off-diagonal terms, that is $i \neq j$ terms. These represent the orthogonality conditions in equation (B.4) which are referred as the linearized admissibility conditions.

These can be written as

$$\sum_{e=1}^{p} \{\phi'\}_j^T [k_e] \{\phi'\}_i \alpha_e = -\{\phi'\}_j^T [k] \{\phi'\}_i, \quad \sum_{e=1}^{p} \{\phi'\}_j^T [m_e] \{\phi'\}_i \alpha_e = -\{\phi'\}_j^T [m] \{\phi'\}_i,$$

$$\text{for } i = 1, ..., n \text{ and } \quad j = i+1, ..., n \tag{B.5}$$

APPENDIX C

Linear Prediction for Eigenvectors

In matrix form, the i th mode free vibration equation for the initial and objective structures can be written as

$$[k]\{\phi\}_i = [m]\{\phi\}_i \omega_i^2 \tag{C.1}$$

$$[k']\{\phi'\}_i = [m']\{\phi'\}_i \omega_i'^2 \tag{C.2}$$

where ω_i^2 is the i th eigenvalue corresponding to the i th eigenvector $\{\phi\}_i$.

Premultiplying equation (C.2) by $\{\phi'\}_i^T$ and using the perturbation relations (2.19)-(2.21) and (B.2), we derive an equation that can be developed into 24 terms among which 15 are nonlinear terms in $[\Delta(\ldots)]^2$ and $[\Delta(\ldots)]^3$.

From this point, we assume small perturbations in order to linearize this equation by keeping the nine linear terms as follows

$$\begin{aligned}
&\{\phi\}_j^T[k]\{\phi\}_i + \{\phi\}_j^T[\Delta k]\{\phi\}_i + \{\phi\}_j^T[k]\{\Delta\phi\}_i + \{\Delta\phi\}_j^T[k]\{\phi\}_i \\
&= \{\phi\}_j^T[m]\{\phi\}_i \omega_i^2 + \{\phi\}_j^T[m]\{\phi\}_i \Delta\omega_i^2 + \{\phi\}_j^T[\Delta m]\{\phi\}_i \omega_i^2 \\
&\quad + \{\phi\}_j^T[m]\{\Delta\phi\}_i \omega_i^2 + \{\Delta\phi\}_j^T[m]\{\phi\}_i \omega_i^2
\end{aligned} \tag{C.3}$$

For $i = j$, using equation (C.1) and its transpose, we get

$$\{\phi\}_i^T[\Delta k]\{\phi\}_i - \{\phi\}_i^T[\Delta m]\{\phi\}_i\omega_i^2 = M_i\Delta\omega_i^2 \tag{C.4}$$

where M_i is the ith diagonal term of the generalized mass matrix defined in (B.1). For $i \neq j$, $\{\phi\}_j^T[m]\{\phi\}_i = 0$ and using the transpose of (C.1) for jth mode, equation (C.3) becomes

$$\{\phi\}_j^T[\Delta k]\{\phi\}_i - \{\phi\}_j^T[\Delta m]\{\phi\}_i\omega_i^2 = \{\phi\}_j^T[m]\{\Delta\phi\}_i(\omega_i^2 - \omega_j^2) \tag{C.5}$$

Assuming that the changes in eigenvectors can be written as

$$[\Delta\Phi] = [\Phi][G]^T \tag{C.6}$$

where [G] is the matrix of admixture coefficients with $G_{ii} = 0$ and G_{ij} small for $i \neq j$. The matrix calculation in (C.6) can be written as

$$\Delta\phi_{i,m} = \sum_{k=1}^{n_r}\phi_{i,k}G_{mk} \tag{C.7}$$

where i corresponds to the degree of freedom and m to the mode vector, can be referred as a reduced basis method. G_{mk} corresponds to the contribution factor of mode k to a change in mode m. Physical meaning of equation (C.7) can be described as follows. For a three dimensional structure, three major mode shapes exists such as stretching, bending and torsional modes. However, one type of mode has little effect on the other modes, which leads to small values of admixture coefficient, G_{ij}.

Substituting equation (C.6) into (C.5), gives

$$G_{ij} = \frac{1}{M_j(\omega_i^2 - \omega_j^2)}(\{\phi\}_j^T[\Delta k]\{\phi\}_i - \{\phi\}_j^T[\Delta m]\{\phi\}_i\omega_i^2) \tag{C.8}$$

Equations (2.21), (C.7) and (C.8) explain the relation between the modes of the initial structure and those of the objective structure.

APPENDIX D

Feasible Sequential Quadratic Programming (FSQP)

This appendix is from the FSQP reference manual [32] by Institute for System Research (ISR), University of Maryland. FSQP is an open source code for minimization of the maximum of a set of smooth objective functions subject to general smooth constraints.

The FSQP algorithm is a superlinearly convergent algorithm for directly tackling optimization problems with multiple linear/nonlinear objective functions (minimax), linear/nonlinear inequality constraints, linear/nonlinear equality constraints.

The general optimization problem can be formulated as follows:

$$\min_{x \in X} \max_{i \in I^f} \{f_i(x)\} \tag{D.1}$$

where $I^f = \{1, \ldots, n_f\}$ and X is the set of points $x \in R^n$ satisfying

$$bl \le x \le bu \quad \text{(boundary constraints)} \tag{D.2}$$

$$G_j(x) \le 0, j = 1, \ldots N_i \quad \text{(nonlinear inequality constraints)} \tag{D.3}$$

$$g_j(x) \le 0, j = 1, \ldots, n_i \quad \text{(linear inequality constraints)} \tag{D.4}$$

$$H_j(x) = 0, j = 1, \ldots, N_e \quad \text{(nonlinear equality constraints)} \tag{D.5}$$

$$h_j(x) = 0, j = 1, \ldots, n_e \quad \text{(linear equality constraints)} \tag{D.6}$$

with $bl \in R^n; bu \in R^n; f_i : R^n \to R, i = 1, \ldots, n_f$ smooth; $G_i : R^n \to R, j = 1, \ldots, N_i$ nonlinear and smooth; $g_i : R^n \to R, j = 1, \ldots, n_i$ linear; $H_i : R^n \to R, j = 1, \ldots, N_e$ nonlinear and smooth; $h_i : R^n \to R, j = 1, \ldots, n_e$ linear. It is allowed to have $n_f = 0$, in which case problem (D.1) is one of finding a point that satisfies a given set of constraints.

Key features related to the present research are as follows:

(1) All nonlinear equality constraints are turned into inequality constraints. Nonlinear equality constraints are changed to inequality constraints and the maximum of the objective function is replaced by an exact penalty function that penalizes nonlinear equality constraint violations only.

(2) Ability to search for an initial feasible point satisfying all linear constraints and nonlinear inequality constraints. That is, it is capable of generating iterations satisfying all linear constraints and nonlinear inequality constraints (mandatory for many applications) starting from a feasible point. If the initial guess provided by the user is infeasible for some inequality constraint or some linear equality constraint, FSQP first generates a feasible point for these constraints; subsequently the successive iterates generated by FSQP all satisfy these constraints.

(3) Ability to improve objective function after each iteration or after at most four iterations (user's option) if there is no nonlinear equality constraints. The user has the option of either requiring that the objective function (penalty function if nonlinear equality constraints are present) decrease at each iteration after feasibility for nonlinear inequality and linear constraints has been reached (monotone line search), or requiring a decrease within at most four iterations (non-monotone line search). The user must provide functions that define the objective functions and constraint functions and may either provide functions to compute the respective gradients or require that FSQP estimate them by forward finite differences.

FSQP is an implementation of two algorithms based on Sequential Quadratic Programming (SQP), modified so as to generate feasible iterates. In the first one (monotone line search), a certain Armijo type arc search is used with property that the step of one is eventually accepted, a requirement for superlinear convergence. In the second one, the same effect is achieved by means of a non-monotone search along a straight line. The merit function used in both searches is the maximum of the objective functions if there is no nonlinear equality constraint, or an exact penalty function if nonlinear equality constraints are present.

BIBLOGRAPHY

1. Cheng G.D., Olhoff N., "An investigation concerning optimal design of solid elastic plates", *International Journal of Solids and Structures*, 1981, 17:305-323.

2. Bendsøe M.P., Kikuchi N., "Generating Optimal Topology in Structural Design Using a Homogenization Method", *Computer Methods in Applied Mechanics and Engineering*, 1988, 71:197-224.

3. Bendsøe M.P., "Optimal Shape Design as a Material Distribution Problem", *Structural and Multidisciplinary Optimization*, 1989, 1: 193-202.

4. Suzuki K., Kikuchi N., "A homogenization method for shape and topology optimization", *Computer Methods in Applied Mechanics and Engineering*, 1991, 93:291-318.

5. Ma Z.D., Kikuchi N., Cheng H.C., "Topological Design for Vibrating Structures", *Computer Methods in Applied Mechanics and Engineering*, 1995, 121:259-280.

6. Pederson N.L., "Maximization of Eigenvalues", *Structural and Multidisciplinary Optimization*, 2000, 20: 2-11.

7. Yang R.J., Chuang C.H., "Optimal Topology Design Using Linear Programming", *Computers and Structures*, 1994, 52-2:265-275.

8. Xie Y.M., Steven G.P., "A Simple Evolutionary Procedure for Structural Optimization", *Computers and Structures*, 1993, 49:885-896.

9. Chu D.N., Xie Y.M., Hira A., and Steven G.P., "Evolutionary Structural Optimization for Problems with Stiffness Constraints", *Finite Elements in Analysis and Design*, 1996, 21(3):239-251.

10. Zhao C., Steven G.P. and Xie Y.M., "Evolutionary Natural Frequency Optimization of Thin Plate Bending Vibration Problems",*Structural Optimization*,1996, 11:244-251.

11. Manickarajah D.,Xie Y.M. and Steven G.P., "An Evolutionary Method for Optimization of Plate Buckling Resistance*", Finite Elements in Analysis and Design*, 1998, 29(3):205-230.

12. Li Q., Steven G.P. and Xie Y.M., "Optimal Shape Design for Steady Heat Conduction by the Evolutionary Procedure", *Inverse Problems in Heat Transfer and Fluid Flow*, 1997, Heat Transfer Div. American Society of Mechanical Engineers, New York, 340:159-164.

13. Querin O.M., Young V., Xie Y.M., Steven GP, "Computational Efficiency and Validation of Bi-directional Evolutionary Structural Optimization", *Computer Methods in Applied Mechanics and Engineering,* 2000, 189:559-573.

14. Proos K.A., Steven G.P., O.M. Querin and Xie Y.M., "Multicriterion Evolutionary Structural Optimization Using the Weighting and the Global Criterion Methods",*AIAA Journal*, 2001, 39(10):2006-2012.

15. Huang X., Xie Y.M., "Convergent and Mesh-independent Solutions for the Bi-directional Evolutionary Structural Optimization Method", *Finite Elements in Analysis and Design*, 2007, 43:1039-1049.

16. Huang X., Xie Y.M., "Bi-directional evolutionary topology optimization of continuum structures with one or multiple materials", *Comput. Mech.*, 2009, 43:393-401.

17. Huang X., Xie Y.M., "Optimal design of periodic structures using evolutionary topology optimization", *Structural and Multidisciplinary Optimization,* 2007, 36(6): 597-606.

18. Stetson K.A., Palma, G.E., "Inversion of First-Order Perturbation Theory and Its Application to Structural Design", *AIAA Journal*, 1976, 14(4):454-460.

19. Sandström R.E., Anderson W.J., "Modal Perturbation Methods for Marine Structures", *SNAME Transactions*, 1982, 90:41-54.

20. Stetson K.A., Harrison I.R., "Redesign of Structural Vibration Modes by Finite Element Inverse Perturbation", *Journal of Engineering for Power*, ASME Transactions, 1981, 103(2): 319-325.

21. Hoff J., Bernitsas M.M., "Dynamic Redesign of Marine Structures", *Journal of Ship Research*, 1985, 29: 285–295.

22. Kim J.H., Bernitsas M.M., "Redesign of Marine Structures", *Marine Structures*, 1990, 1(2):139-183.

23. Bernitsas M.M., Tawekal R.L., "Structural Model Correlation using Large Admissible Perturbation in Cognate Space", *AIAA Journal*, 1991, 29(12):2222-2232.

24. Bernitsas M.M., Rim W., "Redesign of Plates by Large Admissible Perturbations", *AIAA Journal*, 1994, 32: 1021–1028.

25. Bernitsas M.M., Suryatama D., "Structural Redesign by Large Admissible Perturbations with Static Mode Compensation", *Journal of Offshore Mechanics and Arctic Engineering*, 1999, 121(1):39-46.

26. Bernitsas M.M., Blouin V.Y., "Structural Redesign for Forced Response Amplitude with Proportional Damping by Large Admissible Perturbations", *AIAA Journal*, 1999, 37(11):1506-1513.

27. Bernitsas M.M., Kristanto B.K., "Static Stress Redesign of Structures by Large Admissible Perturbations", *Journal of Offshore Mechanics and Arctic Engineering*, 2003, 127:122-129.

28. Blouin V.Y., Bernitsas M.M., "Cognate Space Identification for Forced Response Structural Redesign", *Journal of Offshore Mechanics and Arctic Engineering*, 2005, 127(3):227-233.

29. Suryatama D., Bernitsas M.M., "Topology and Performance Redesign of Complex Structures by Large Admissible Perturbations", *Structural and Multidisciplinary Optimization*, 2000, 20:138-153.

30. Miao L., Bernitsas M.M., "Topology Redesign for Performance by Large Admissible Perturbations", *Structural and Multidisciplinary Optimization*, 2006, 31:117-133.

31. Earmme T., Bernitsas M.M., "Parametric Evolution of Structural Topology by Large Admissible Perturbations", *7th World Congress of Structural and Multidisciplinary Optimization*, 2007, Seoul Korea.

32. Zhou, J.L.,Tits, A.L. and Lawrence, C.T., *User's Guide for FFSQP Version 3.7:A FORTRAN Code for Solving Constrained Nonlinear (Minimax) Optimization Problems, Generating Iterates Satisfying All Inequality and Linear Constraints*, Electrical Engineering Department and Institute of Systems Research, University of Maryland, College Park. MD 20742, 1997.

33. *MSC/NASTRAN Version 70.0 Advanced Dynamics User's Guide*, MacNeal-Schwandler Corporation, Los Angeles, CA., November 1989.